



UNIVERSITY COLLEGE CORK

DEPARTMENT OF PHYSICS

Module PY4115 (Major Research Project)

Final Report

**Exotic State Preparation in a
Triangular Optical Lattice**

Cian M. Roche

115535053


Supervised by

Dr. Anthony Kiely

April 15, 2019

Declaration

This report was written entirely by the author, except where stated otherwise. The source of any material not created by the author has been clearly referenced. The work described in this report was conducted by the author, except where stated otherwise.

Signed:  _____

April 15, 2019

Abstract

Optical lattices provide highly controllable systems for trapping and exciting gases of ultracold atoms. They are ideal candidates for the quantum simulation of condensed matter systems, for which many implementations require higher orbital occupation. In this report, methods for creating higher orbital states in a square optical lattice are extended to the triangular lattice geometry, where the lattice sites are assumed to be singly occupied by ultracold atoms in the Mott regime. The target states are achieved using three techniques: (i) modulation of the positions of the trap minima (known as shaking), (ii) modulation of the polarisation phase between the lasers forming the lattice and (iii) amplitude modulation of the control lasers. Specific control sequences are designed to achieve both selective excitation of atoms to higher orbital states and a large-angular-momentum state in which each atom has orbital angular momentum $l \simeq 2\hbar$. Although the target states designed are specific, the techniques developed in this report are general and can be used to create a wide variety of states.

Acknowledgments

I would like to thank my supervisor Dr. Anthony Kiely, for his mentorship, patience and far too much of his time.

Contents

1	Introduction	1
2	Background	4
3	Triangular Lattice Potential	5
3.1	Interference Between Control Lasers	6
3.2	Lattice Geometry	7
4	Generating Excited States	8
4.1	Lattice Shaking	9
4.1.1	Shaking Schemes	9
4.1.2	Reference Frame Transformation	10
4.1.3	Four-level Approximation	11
4.1.4	Pulse Sequences	15
4.2	Modulation of Polarization Phase	17
4.2.1	Four-level Approximation	17
4.2.2	Selective Site excitation	18
4.3	Amplitude Modulation	21
4.3.1	Alternative Lattice Potential	21
4.3.2	Four-level Approximation	23
4.3.3	Control Scheme	27
5	Discussion	29
6	Conclusions	32
	References	33
A	Eigenstate Parity Restriction	36
B	Eigenstates of Unperturbed Hamiltonian	37
C	Population Transfer Pulses	38
D	Unitary Transformations	40

List of Figures

1	(a) Contour plot representation of a square lattice, named so because of its square unit cell in two dimensions (red). (b) 3D plot of the same optical lattice.	2
2	Laser arrangement to form triangular optical lattice	5
3	Triangular lattice geometry, where $2L \equiv 2\pi/\sqrt{3}k$ is the nearest neighbour spacing.	8
4	Four-level scheme of first excited states and the coupling parameters between them.	12
5	(a) State evolution for particle initially in state $ 00\rangle$ under influence of π pulse in Ω_y (b) Shaking amplitude corresponding to this π pulse.	16
6	(a) State evolution for particle initially in state $ 00\rangle$ under influence of π pulse in Ω_x followed by $\pi/2$ pulse in Ω_y (b) Shaking amplitude corresponding to this π pulse.	17
7	(a) Change in sign of interference term at different bands of lattice sites (if interference term is positive along red bands then it is negative along blue) (b) $V_\rho(t)$ with ramp-up time $\tau = T/10$	19
8	(a) State evolution for particle initially in state $ 00\rangle$ under influence of π pulse in Ω_x (b) State evolution on lattice site where interference term is effectively “turned off” via interference term modulation.	21
9	Four-level scheme of second excited states and the coupling parameters between them.	24
10	(a) Bessel functions of the first kind. (b) Parameters A_{mq} and C_{2002} as a function of lattice depth.	26
11	State evolution for particle initially in state $ 00\rangle$ under influence of π pulse in Ω_y and a $-\pi/2$ pulse in Ω_c to achieve target state $ +\rangle$. (b) Amplitude modulation corresponding to this control sequence.	28
12	Comparison of rotating wave approximation in accurate regime and when the assumption breaks down	30
13	Fidelity $ \langle \Psi_b \psi(T) \rangle ^2$ dependence on total process time T	31

List of Abbreviations

Abbreviation	Meaning
Sec.	Section
Eq.	Equation
Fig.	Figure
2D	Two-dimensional
3D	Three-dimensional

List of Scientific Symbols

Symbol	Meaning	Symbol	Meaning
Boldface	vector quantity	Δ	Detuning in frequency
m	Meters	\mathbf{r}	Position vector
a.m.u.	Atomic mass units	\mathbf{R}_0	Position vector of central lattice minimum
K	Kelvin	X	Cartesian x component of \mathbf{R}_0
ms	Milliseconds	Y	Cartesian y component of \mathbf{R}_0
V	Potential energy function	H	Hamiltonian
\mathbf{E}	Electric field	\mathbf{p}	Quantum mechanical momentum operator
\mathbf{k}	Wave vector	m	Mass
e	Eulers number	U	Unitary operator
i	Imaginary unit $\sqrt{-1}$	Ω	Rabi frequency
ρ	Polarization phase	$ \psi\rangle$	Quantum state of system in bra-ket notation
\hbar	Reduced Planck constant	ψ	Wave function of system in position representation
$\boldsymbol{\mu}$	Transition dipole moment		
t	Time		
ϕ	Spatial phase angle		
ω	Angular frequency		

1 Introduction

An optical lattice is an artificial crystal of light created by interfering laser beams. When an atom is illuminated by a laser beam, the electric field of the laser induces a dipole moment in the atom which couples to the field and modifies the internal states of the atom. This interaction (called the AC-Stark shift) depends on the light intensity and thus a spatially varying intensity produces a spatially varying potential which can be used to trap atoms. The interference pattern formed by the interference of more than one retroreflected laser beam in a plane produces a 2D periodic potential landscape we call an optical lattice. This potential is periodic in space and stationary in time because retroreflected laser beams form standing waves that vary in space only.

The control parameters of the lasers (eg. amplitude, phase, polarization) can be changed in time to precisely control aspects of the lattice such as the spacing between adjacent lattice sites (known as the lattice constant) and the potential well depth. Condensed matter systems such as crystals are often grown and prone to imperfections and vibrational modes of the lattice itself, but optical lattices are formed via the interference of light and are therefore perfectly regular and cannot be deformed by vibrations. This high degree of control and perfect periodicity makes optical lattices invaluable as tools in quantum simulation, where there is a direct mapping from the crystal structure of the condensed matter system to the optical lattice itself and from the conduction electrons of the solid state system to the atoms trapped in the optical lattice [1]. The atoms trapped in an optical lattice mimic the behaviour of these conduction electrons in an ionic crystal, but in a highly-controllable and stable environment. Note that the energetic and spatial scales involved in this simulated system are far different from those of a condensed matter system, as summarised by the following table:

	Optical Lattice	Solid State Crystal
Trapped particle	Neutral Atoms	Valence Electrons
Lattice spacing	$\sim 10^{-6}$ m	$\sim 10^{-10}$ m
Particle mass	10 – 100 a.m.u.	10^{-3} a.m.u.
Temperature	$\sim 10^{-9}$ K	~ 100 K

Table 1: Summary of the mapping from a condensed matter system to an optical lattice and the length, energy and mass scales involved in both regimes. Orders of magnitude obtained from [2].

The large difference in temperature is a result of the difference in lattice spacing and mass of the trapped particles, such that to probe the same physics that occurs at 100 K in a solid state system we require a temperature on the order of a few nK in an optical lattice. Of course this extreme cooling presents its own challenges, but also comes with advantages such as very low thermal noise and relatively long timescales for observations (ms to seconds). Studies of ultracold atoms in optical lattices have primarily been conducted with the square lattice geometry (see Fig. 1) due to its simplicity and wide variety of applications, but in order to accurately simulate condensed matter systems with triangular or hexagonal lattice geometries, corresponding triangular or hexagonal optical lattices are required. An optical lattice formed via the interference of three or more lasers such as the triangular lattice will not in general be separable¹ and therefore more difficult to analyze, but despite this some studies have been conducted with these geometries [3][4][5].

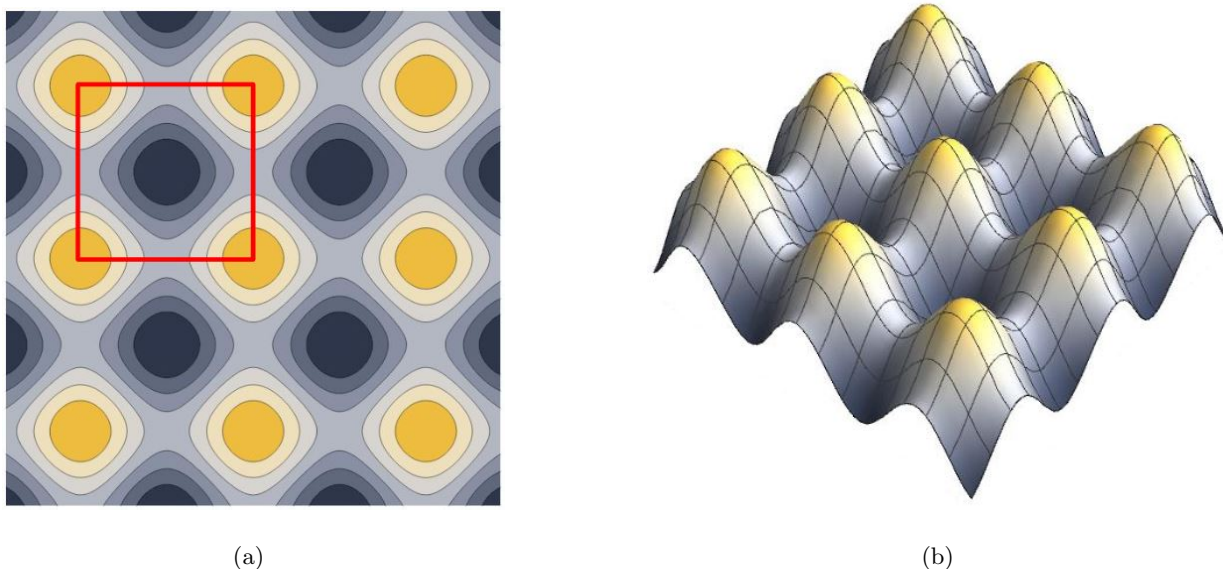


Figure 1: (a) Contour plot representation of a square lattice, named so because of its square unit cell in two dimensions (red). (b) 3D plot of the same optical lattice.

Typically an ultracold gas of atoms will be loaded into an optical lattice in the ground state, but as outlined in the next section many applications of optical lattices require higher orbital occupancy. In this project, we take the geometry of a triangular lattice formed by the retroreflection of three lasers and develop techniques of exciting the trapped atoms to higher orbitals. We assume the lattice

¹“Separable” means that the potential can be written as a product of potentials in the different spatial coordinates of the system. For example if the coordinates used are 2D polar coordinates r and θ , then a potential separable in these coordinates could be written $V(r, \theta) = R(r)\Theta(\theta)$

sites to be singly occupied (ie a filling factor of one) and that we work in the Mott regime such that we neglect interactions between particles localized in different lattice sites. We also assume a strong confinement in the direction orthogonal to the plane of lattice confinement and therefore neglect dynamics in this dimension. The techniques of excitation investigated here are

- (i) Lattice shaking, whereby the spatial phases of the control lasers are varied so as to translate the whole optical lattice without deformation.
- (ii) Modulation of the polarization phase of the lasers, a method of modulating the interference terms between the control lasers either to provide energy/ angular momentum to the atoms in each lattice site or to selectively excite certain lattice sites, as is done in this report.
- (iii) Modulation of control laser amplitudes, whereby the amplitude of the control lasers (and thus the depth of the potential well at each lattice site) is varied in time.

The rest of the report is structured as follows: In the next section, we will outline the major results achieved using optical lattices in the past two decades, in order to motivate the need for further research and demonstrate the versatility of this tool. In section 3, we derive the potential structure from first principles and outline methods of controlling the interference terms between the lasers forming the lattice. In section 4, for each of the three methods outlined above we first derive a four-level approximation for the system, then use this four-level approximation to derive control schemes (the control parameters of the lasers as functions of time) that bring the system to example target states. In section 5, approximations made in the four-level approximations are verified and experimental considerations for creating states using these control schemes are discussed. In section 6, the results of the four-level schemes are summarised and their usefulness put into perspective, with some useful derivations and explanations present in the Appendix.

2 Background

It was pointed out in 1997 that a metal-insulator-like transition can be induced in ultracold atoms in a quasiperiodic optical potential by changing the amplitude of the driving force in time [6]. In 2002 an optical lattice was used to observe the quantum phase transition from a superfluid to a Mott insulator in a gas of ultracold atoms [7], which sparked great interest in the field. Since then the study of ultracold atoms in optical lattices has grown rapidly as an invaluable tool in quantum simulation. For example, both cold non-condensed atoms [8][9] and Bose-Einstein condensates [10][11] have been studied in optical lattices under the action of both a time-independent homogeneous force and a time-periodic force.

In experiments using optical lattices typically the lattice is two-dimensional and the third dimension is made redundant with a harmonic confinement. Note that this (along with the Gaussian profile of the lasers) causes an inhomogeneity in the lattice that must be taken into account when comparing experimental results to results derived for a perfectly periodic potential [12]. A gas loaded into the trap is cooled to temperatures on the order of nK via methods such as evaporative and laser cooling, which greatly reduces thermal noise. A detailed review of theoretical and experimental work in optical lattices can be found at [12] and a more modern summary at [13].

There is great interest in the scientific community surrounding the study of condensed matter systems with high orbital occupancy. Reasons for this include the important role higher orbital electrons play in models of high temperature superconductivity [14][15] and their proposed role in quantum computation [16]. The orbital physics of electrons can be emulated in an optical lattice using the orbital degrees of freedom in the higher Bloch bands of the lattice [17][18], leading to great interest in studying these bands [19]. As a result of this interest, extensive research has been conducted in the field of creating excited states in optical lattices, primarily in the modulation of lattice amplitudes and the positions of trap minima (shaking). Lattice shaking has been implemented experimentally [20][8] and has been used to realize theoretical models such as the Haldane model, which is the first crystal model to describe topological behaviour [21]. Periodic modulation of the lattice amplitude has also been used to prepare higher orbital states in an optical lattice, and was used to study the Bose-Hubbard model [10]. In this report we develop these excitation techniques, in a lattice geometry suitable for studying triangular condensed matter systems.

3 Triangular Lattice Potential

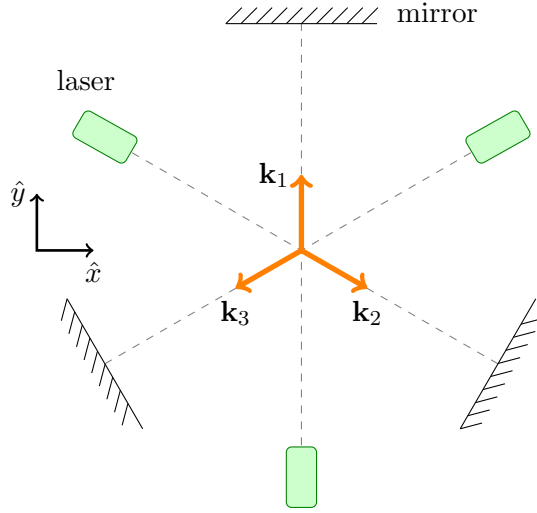


Figure 2: Laser arrangement to form triangular optical lattice

Consider the interference of three retro-reflected laser beams as in Fig. 2 such that each laser establishes a standing wave. Each laser is assumed to have a variable phase angle $\phi(t)$ and polarisation phase $\rho(t)$. The net electric field \mathbf{E} at some position \mathbf{r} is given by the superposition of the three electric fields at that point, due to the linear nature of Maxwell's equations;

$$\mathbf{E}(\mathbf{r}, t) = \sum_{j=1}^3 \mathbf{E}_j e^{i\rho_j(t)} \sin[\mathbf{k}_j \cdot \mathbf{r} + \phi_j(t)] e^{-i\omega_L t}, \quad (1)$$

where ω_L is the common frequency of each laser. The wave vectors \mathbf{k}_j as shown in Fig. 2 are rotated by an angle of $2\pi/3$ radians relative to each other and are represented in Cartesian coordinates by

$$\mathbf{k}_1 = k \begin{bmatrix} 0 \\ 1 \end{bmatrix}, \quad \mathbf{k}_2 = \frac{k}{2} \begin{bmatrix} \sqrt{3} \\ -1 \end{bmatrix}, \quad \mathbf{k}_3 = \frac{k}{2} \begin{bmatrix} -\sqrt{3} \\ -1 \end{bmatrix}, \quad (2)$$

where k is the common wavenumber of each laser. For simplicity we assume that all polarisations are of the same magnitude and direction², ie $\mathbf{E}_1 = \mathbf{E}_2 = \mathbf{E}_3 \equiv \mathbf{E}_0$. The potential experienced by an atom with transition dipole moment $\boldsymbol{\mu}$ in a two dimensional optical lattice [23] is given by

$$V(\mathbf{r}, t) = \frac{1}{4\hbar\Delta} |\boldsymbol{\mu} \cdot \mathbf{E}^*(\mathbf{r}, t)|^2, \quad (3)$$

wherein Δ is the detuning of the lasers with respect to the atomic transition frequencies. If the energy of an atomic transition is $\hbar\omega_0$, then using lasers tuned above this resonance frequency (ie

²Note that choosing the polarizations to be in the plane of the lattice can be used to create a hexagonal lattice structure, for details see [22].

$\omega_L > \omega_0$) is called “blue” detuning. Conversely, $\omega_L < \omega_0$ is called “red” detuning. The quantity Δ is defined as $\omega_L - \omega_0$ and is therefore positive in the case of blue detuning. The laser detuning is assumed here to be blue. Combining Eq. 1 and Eq. 3 we obtain

$$\begin{aligned}
V(\mathbf{r}, t) = & V_0 \sin^2[\mathbf{k}_1 \cdot \mathbf{r} + \phi_1(t)] + V_0 \sin^2[\mathbf{k}_2 \cdot \mathbf{r} + \phi_2(t)] + V_0 \sin^2[\mathbf{k}_3 \cdot \mathbf{r} + \phi_3(t)] \\
& + 2V_0 \cos[\rho_2(t) - \rho_1(t)] \sin[\mathbf{k}_1 \cdot \mathbf{r} + \phi_1(t)] \sin[\mathbf{k}_2 \cdot \mathbf{r} + \phi_2(t)] \\
& + 2V_0 \cos[\rho_3(t) - \rho_1(t)] \sin[\mathbf{k}_1 \cdot \mathbf{r} + \phi_1(t)] \sin[\mathbf{k}_3 \cdot \mathbf{r} + \phi_3(t)] \\
& + 2V_0 \cos[\rho_3(t) - \rho_2(t)] \sin[\mathbf{k}_2 \cdot \mathbf{r} + \phi_2(t)] \sin[\mathbf{k}_3 \cdot \mathbf{r} + \phi_3(t)],
\end{aligned} \tag{4}$$

where we have defined

$$V_0 \equiv \frac{|\boldsymbol{\mu} \cdot \mathbf{E}_0|^2}{4\hbar\Delta}. \tag{5}$$

This can be rewritten in a more compact form as

$$V(\mathbf{r}, t) = V_0 \sum_{i=1}^3 \sum_{j=1}^3 \cos[\rho_i(t) - \rho_j(t)] \sin[\mathbf{k}_i \cdot \mathbf{r} + \phi_i(t)] \sin[\mathbf{k}_j \cdot \mathbf{r} + \phi_j(t)]. \tag{6}$$

3.1 Interference Between Control Lasers

The potential Eq. 6 is relatively complicated, and so we seek here to simplify it by removing all interference terms between different control lasers. Note the distinction between interference between different lasers and the control lasers interfering with their retroreflected beams, which is necessary to create a lattice stationary in time. To accomplish this, we first detune the frequency of laser 1 (corresponding to \mathbf{k}_1) by some amount ϵ . The time dependence of the components of lasers 2 and 3 will be $e^{-i\omega_L t}$, whereas for laser 1 this will now be $e^{-i(\omega_L + \epsilon)t}$. Via the same calculation as the previous section we obtain

$$\begin{aligned}
V(\mathbf{r}, t) = & V_0 \sin^2(\mathbf{k}_1 \cdot \mathbf{r} + \phi_1) + V_0 \sin^2(\mathbf{k}_2 \cdot \mathbf{r} + \phi_2) + V_0 \sin^2(\mathbf{k}_3 \cdot \mathbf{r} + \phi_3) \\
& + 2V_0 [\cos(\rho_2) \cos(\epsilon t) + \sin(\rho_2) \sin(\epsilon t)] \sin(\mathbf{k}_1 \cdot \mathbf{r} + \phi_1) \sin(\mathbf{k}_2 \cdot \mathbf{r} + \phi_2) \\
& + 2V_0 [\cos(\rho_3) \cos(\epsilon t) + \sin(\rho_3) \sin(\epsilon t)] \sin(\mathbf{k}_1 \cdot \mathbf{r} + \phi_1) \sin(\mathbf{k}_3 \cdot \mathbf{r} + \phi_3) \\
& + 2V_0 \cos(\rho_3 - \rho_2) \sin(\mathbf{k}_2 \cdot \mathbf{r} + \phi_2) \sin(\mathbf{k}_3 \cdot \mathbf{r} + \phi_3),
\end{aligned} \tag{7}$$

where we have omitted the explicit time dependence of the control parameters ρ and ϕ . We then impose the condition that for a control scheme of total time T , we have $\omega_L \gg \epsilon \gg 1/T$. The first part of this condition ensures that the lattice be only negligibly distorted by the shift in frequency,

while the second ensures that interference terms containing ϵt oscillate sufficiently quickly to average to zero [24]. Thus we are left with the triangular lattice potential

$$V(\mathbf{r}, t) = V_0 \sin^2(\mathbf{k}_1 \cdot \mathbf{r} + \phi_1) + V_0 \sin^2(\mathbf{k}_2 \cdot \mathbf{r} + \phi_2) + V_0 \sin^2(\mathbf{k}_3 \cdot \mathbf{r} + \phi_3) + V_\rho(t) \sin(\mathbf{k}_2 \cdot \mathbf{r} + \phi_2) \sin(\mathbf{k}_3 \cdot \mathbf{r} + \phi_3), \quad (8)$$

where we have defined the control parameter

$$V_\rho(t) \equiv 2V_0 \sin[\rho(t)]. \quad (9)$$

The quantity $\rho(t)$ describes the deviation from orthogonal polarisation between control lasers 2 and 3 via $\rho(t) \equiv \rho_3(t) - \rho_2(t) + \pi/2$, such that if control lasers 2 and 3 are orthogonally polarised this interference term will be zero³. This is the assumption made in the following section in which we consider only the lattice shaking, leaving us with the potential

$$V(\mathbf{r}, t) = V_0 \sin^2(\mathbf{k}_1 \cdot \mathbf{r} + \phi_1) + V_0 \sin^2(\mathbf{k}_2 \cdot \mathbf{r} + \phi_2) + V_0 \sin^2(\mathbf{k}_3 \cdot \mathbf{r} + \phi_3). \quad (10)$$

3.2 Lattice Geometry

The optical lattice as defined by Eq. 10 exhibits a nearest-neighbour spacing of $2L \equiv 2\pi/\sqrt{3}k$ (which happens to be in directions perpendicular to the \mathbf{k}_j) and a distance between the lattice minima of $2\pi/k$ along directions parallel to the \mathbf{k}_j . This lattice structure is shown in Fig. 3.

Let us define a set of vectors $\{\mathbf{k}_1^\perp, \mathbf{k}_2^\perp, \mathbf{k}_3^\perp\}$, which are simply each of the \mathbf{k}_j rotated counter-clockwise by $\pi/2$ radians as in Fig. 3. These vectors will be useful in describing dynamics at different lattice sites and are represented in Cartesian coordinates by

$$\mathbf{k}_1^\perp = k \begin{bmatrix} -1 \\ 0 \end{bmatrix}, \quad \mathbf{k}_2^\perp = \frac{k}{2} \begin{bmatrix} 1 \\ \sqrt{3} \end{bmatrix}, \quad \mathbf{k}_3^\perp = \frac{k}{2} \begin{bmatrix} 1 \\ -\sqrt{3} \end{bmatrix}. \quad (11)$$

We assume the extent of the unit cell to be roughly described by $x \in \{-L, L\}$, $y \in \{-L, L\}$, ie a Cartesian square of side length $2L$. Since we assume the system to be in the Mott regime, all integrals that appear in calculations in later sections (for example $\langle \Phi | \cos(kx) | \Phi \rangle$ where $|\Phi\rangle$ is a state of the system) will be taken over the domain of the unit cell, as opposed to over all space.

³In general, orthogonally polarized waves will not interfere. This is the first of the Fresnel Arago laws which describe the interference properties of light with different states of polarization [25].

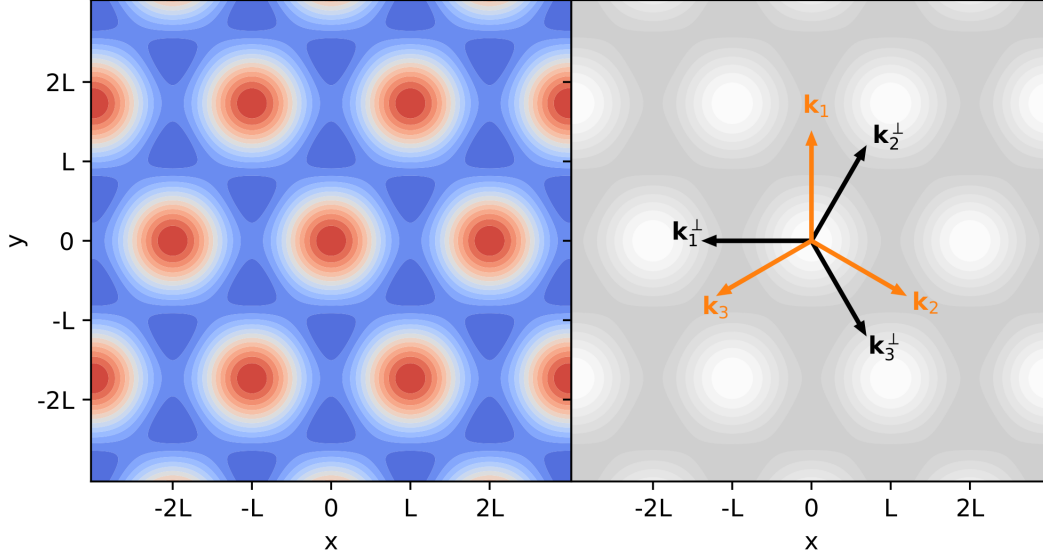


Figure 3: Triangular lattice geometry, where $2L \equiv 2\pi/\sqrt{3}k$ is the nearest neighbour spacing.

4 Generating Excited States

We will now examine three methods of generating excited states in this triangular optical lattice. In each case we will derive a four-level approximation for the Hamiltonian of a particle in one of the lattice sites, then use this approximation to derive control schemes (the control laser parameters as functions of time) that bring the system to some desired target state. The four-level approximations are necessary as our problem is a very difficult one to solve: given the evolution of the system from the ground state to some desired target state, solve for the time-dependence of the functions involved in the potential. Here these functions are the control parameters for our lasers forming the lattice, such as amplitude and phase. The methods described here are general and could be used in many optical lattice geometries, but the control sequences designed in the following sections apply only to their respective lattice potentials and target states.

4.1 Lattice Shaking

4.1.1 Shaking Schemes

By manipulating the $\phi_j(t)$ we can shake the whole lattice along any desired direction, but since the potential is not separable in x and y as with a square lattice, certain relationships must hold between the ϕ_j for the lattice to remain undistorted. If we denote the time-dependent x and y coordinates of the central minimum by $X(t)$ and $Y(t)$ respectively, the ϕ_i can be written in terms of X and Y as

$$\phi_1 = -kY \quad (12)$$

$$\phi_2 = -\frac{\sqrt{3}}{2}kX + \frac{1}{2}kY \quad (13)$$

$$\phi_3 = \frac{\sqrt{3}}{2}kX + \frac{1}{2}kY, \quad (14)$$

where the explicit form Eq. 2 of the \mathbf{k}_j has been used in the evaluation of $\mathbf{r} \cdot \mathbf{k}_j$ and we omit the explicit time dependence of X, Y and the ϕ_j . We can then write V explicitly in terms of the translations X and Y as

$$\begin{aligned} V(\mathbf{r} - \mathbf{R}_0, t) = & V_0 \cos^2[k(y - Y)] + V_0 \cos^2 \left[k \frac{\sqrt{3}}{2}(x - X) - \frac{k}{2}(y - Y) \right] \\ & + V_0 \cos^2 \left[-k \frac{\sqrt{3}}{2}(x - X) - \frac{k}{2}(y - Y) \right] \end{aligned} \quad (15)$$

where \mathbf{R}_0 is the time dependent position of the central minimum (X, Y) , where the notation $\mathbf{v} = (a, b)$ implies $\mathbf{v} = a\hat{x} + b\hat{y}$. This leads to three natural choices for lattice shaking directions, namely (a) along \hat{x} , which would imply $Y = 0$ (b) along \hat{y} , which would imply $X = 0$ and (c) along the line $y = x$, which would imply $X = Y$. Therefore we have the constraints for each scheme

$$\begin{aligned} \text{(a)} \quad & \phi_1 = 0, & \phi_2 = -\frac{\sqrt{3}}{2}kX, & \phi_3 = -\phi_2 \\ \text{(b)} \quad & \phi_1 = -kY, & \phi_2 = \frac{1}{2}kY, & \phi_3 = \phi_2 \\ \text{(c)} \quad & \phi_1 = -kY, & \phi_2 = -\frac{1}{2}(\sqrt{3} - 1)kY, & \phi_3 = \frac{1}{2}(\sqrt{3} + 1)kY \end{aligned} \quad (16)$$

where X and Y (and thus, the ϕ_i) are arbitrary functions of time, such that the lattice can be shaken with any time dependence along any direction desired, via a linear combination of (a) and (b) in Eq. 16.

4.1.2 Reference Frame Transformation

We now examine the Hamiltonian for a particle in the central lattice site at $(0,0)$, although at this level of analysis all atoms will evolve identically. It is useful to transform the Hamiltonian of the particle from the lab frame to the lattice rest frame, in which the lattice is at rest and the particle is shaken by the $\phi_j(t)$. This transformation is given in [8] and is summarised here. The lab Hamiltonian is given by

$$H_{\text{lab}}(t) = \frac{\mathbf{p}^2}{2m} + V(\mathbf{r} - \mathbf{R}_0, t) \quad (17)$$

To transform to the lattice rest frame, we utilise a unitary operator $U = U_3 U_2 U_1$ where each of the U_j are themselves unitary operators. The first is a translation operator

$$U_1 = \exp \left[\frac{i}{\hbar} \mathbf{R}_0(t) \cdot \mathbf{p} \right], \quad (18)$$

the second is a momentum shift operator (where an upper dot represents a time derivative)

$$U_2 = \exp \left[-\frac{i}{\hbar} m \dot{\mathbf{R}}_0(t) \cdot \mathbf{r} \right], \quad (19)$$

and third an operator which removes a time dependent energy shift from the Hamiltonian,

$$U_3 = \exp \left[-\frac{i}{\hbar} \frac{m}{2} \int_0^t ds \dot{\mathbf{R}}_0(s) \cdot \dot{\mathbf{R}}_0(s) \right] \quad (20)$$

The Hamiltonian changes under any unitary transformation U_0 as $H_{\text{new}} = U_0^\dagger H_{\text{old}} U_0 - i\hbar U_0^\dagger \dot{U}_0$ [26]. Therefore the lattice frame Hamiltonian is given by

$$H_{\text{lattice}}(t) = U^\dagger H_{\text{lab}} U - i\hbar U^\dagger \dot{U}. \quad (21)$$

Evaluating Eq. 21 and making use of Liebniz's integral rule we obtain

$$H_{\text{lattice}}(t) = \frac{\mathbf{p}^2}{2m} + V(\mathbf{r}, t) + m \ddot{\mathbf{R}}_0 \cdot \mathbf{r} \quad (22)$$

The advantage of this transformation is that the Hamiltonian of the system in question here is now easily written as the sum of a time-independent part H_0 and a time-dependent part $H_1(t)$, ie $H_{\text{lattice}}(t) = H_0 + H_1(t)$ with⁴

$$H_0 \equiv \frac{\mathbf{p}^2}{2m} + V_0 \sin^2(\mathbf{k}_1 \cdot \mathbf{r}) + V_0 \sin^2(\mathbf{k}_2 \cdot \mathbf{r}) + V_0 \sin^2(\mathbf{k}_3 \cdot \mathbf{r}), \quad (23)$$

$$H_1(t) \equiv m \ddot{X}x + m \ddot{Y}y. \quad (24)$$

⁴Note that the form of $H_1(t)$ will change in later sections as we consider different techniques, but the unperturbed Hamiltonian H_0 will remain the same throughout the report.

The time-dependent part of this Hamiltonian has an intuitive form, as in the lattice frame \ddot{X} represents the acceleration of the particle in \hat{x} , and therefore $m\ddot{X}$ represents the force on the particle and $m\ddot{X}x$ a potential energy.

4.1.3 Four-level Approximation

As mentioned before, we now have the following problem to solve: We have a time-dependent Hamiltonian and an atom in the ground state, then we choose a target state and must solve for the time dependence of the potential that accomplishes this. This is not possible to do in general with the full Hamiltonian Eq. 23 and so we use a basis of only the four most relevant states of the system to obtain an approximation for the dynamics. We use a basis of only four states because these states are resonantly coupled, but due to the anharmonicity⁵ of the potential higher states are slightly detuned in energy and can therefore be neglected. This idea is further developed in Sec. 5. The basis states chosen are $\{|00\rangle, |10\rangle, |01\rangle, |11\rangle\}$, where in this notation, $\langle \mathbf{r} | ij \rangle = \Phi_i(x)\Phi_j(y)$ and Φ denotes a local eigenstate of H_0 in one dimension as outlined in Appendix B. For example, $|01\rangle$ describes a state which is a product of the 1D ground state of H_0 in x and the 1D first excited state of H_0 in y . The energies of the eigenstates are given by $E_{ij} = \hbar\omega_{ij}$, with the energy gap between the ground state and first excited state given by $E_{10} - E_{00} \equiv \hbar\omega_d$ as in Fig. 4. This energy gap is important as if we wish to transfer an atom from the ground state to the first excited state we can do so by varying the control parameters on-resonance with this transition (ie at a frequency ω_d) as we will do in the following calculations.

Note that since H_0 is not separable in x and y , it is not possible to write its eigenstates as products of functions $\Phi_i(x)\Phi_j(y)$ as is done above. This approach does however become exact in the harmonic limit $V_0 \rightarrow \infty$ and is useful to obtain an approximation for the dynamics of the system. The validity of using a four-level scheme comprised of states separable in x and y is discussed in Appendix B.

⁵In a quantum harmonic oscillator, all energy levels are equally spaced by $\hbar\omega$ where ω is the natural frequency of the oscillator. In this case a process that excites particles from the ground state to the first excited state will also excite atoms in the first excited state to the second excited state, because the energy gap is identical. This leads to “leakage” of the state of the particle to higher levels, which makes a perfectly harmonic trap not suitable for the preparation of higher orbital states.

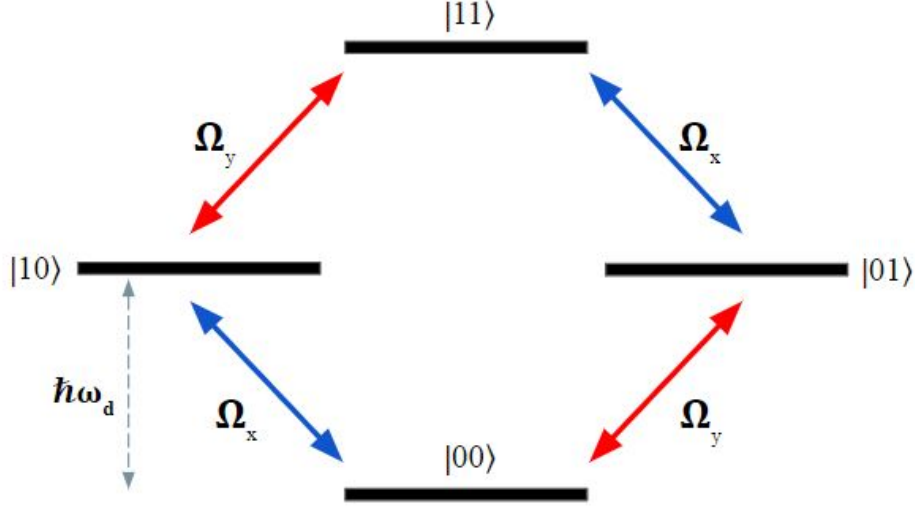


Figure 4: Four-level scheme of first excited states and the coupling parameters between them.

We now assume a particular form of the lattice shaking, chosen here to be

$$X(t) = -g_x(t) \cos(\omega_d t), \quad (25)$$

$$Y(t) = -g_y(t) \cos(\omega_d t), \quad (26)$$

which assumes the frequency of the shaking is on resonance with the energy transition from the ground state to first excited state. Defining two new functions

$$f_x^{(1)}(t) \equiv m\ddot{X} = m\omega_d^2 g_x(t) \cos(\omega_d t), \quad (27)$$

$$f_y^{(1)}(t) \equiv m\ddot{Y} = m\omega_d^2 g_y(t) \cos(\omega_d t), \quad (28)$$

where we have assumed $g_x(t)$ and $g_y(t)$ vary slowly in time, we can write the time dependent part of the Hamiltonian as

$$H_1(t) = x f_x^{(1)}(t) + y f_y^{(1)}(t). \quad (29)$$

We now define a unitary transformation $\mathcal{U}(t)$ whose purpose is to remove all diagonal terms in the Hamiltonian. If this is achieved we have a clear representation of the coupling (population transfer) between the different basis eigenstates of the system via the off-diagonal elements of the matrix representation of the lattice Hamiltonian. If \mathcal{U} is defined as

$$\begin{aligned} \mathcal{U}(t) \equiv & e^{-i\omega_{00}t} \mathcal{X}_{00}(t) |00\rangle \langle 00| + e^{-i\omega_{10}t} \mathcal{X}_{10}(t) |10\rangle \langle 10| \\ & + e^{-i\omega_{01}t} \mathcal{X}_{01}(t) |01\rangle \langle 01| + e^{-i\omega_{11}t} \mathcal{X}_{11}(t) |11\rangle \langle 11|, \end{aligned} \quad (30)$$

with the quantities $\mathcal{X}_{n,m}(t)$ defined as

$$\mathcal{X}_{nm} \equiv \exp\left(-\frac{i}{\hbar} \int_0^t ds \langle nm | H_1(s) | nm \rangle\right), \quad (31)$$

then this goal is accomplished. Note that only diagonal matrix elements of H_1 are involved in the \mathcal{X} as these are the elements we wish to “transform away”. The quantity $\langle nm | H_1(s) | nm \rangle$ which appears in the \mathcal{X}_{nm} simplifies greatly in this case, as all terms in $H_1(t)$ are odd with respect to x or y . Since the overlaps always contain two identical states in either x or y , only even terms in $H_1(t)$ would be nonzero regardless of the parity of the eigenstates in question. This becomes clear when a general separable term $F(x, y) = F_x(x)F_y(y)$ in $\langle nm | H_1(s) | nm \rangle$ is expanded as

$$\langle nm | F_x(x)F_y(y) | nm \rangle = \int_{-L}^{+L} dx \Phi_n(x)F_x(x)\Phi_n(x) \int_{-L}^{+L} dy \Phi_m(y)F_y(y)\Phi_m(y). \quad (32)$$

Therefore in this case, all \mathcal{X} reduce to 1. In a four state basis the Hamiltonian will be represented by a 4×4 matrix which we will denote $H_{4L}(t)$, and as with any unitary transformation the Hamiltonian changes under \mathcal{U} as $H_{4L}(t) = \mathcal{U}^\dagger H_0 \mathcal{U} - i\hbar \mathcal{U}^\dagger \dot{\mathcal{U}} + \mathcal{U}^\dagger H_1(t) \mathcal{U}$. If we exploit the fact that for a symmetric potential structure ground state wave functions $\Phi_0(s)$ are even, whilst first excited state wave functions $\Phi_1(s)$ are odd (shown in Appendix A) and the orthogonality of the eigenstates of the Hamiltonian H_0 the first two terms simplify to

$$\mathcal{U}^\dagger H_0 \mathcal{U} - i\hbar \mathcal{U}^\dagger \dot{\mathcal{U}} = - \sum_j |j\rangle \langle j| H_1(t) |j\rangle \langle j|, \quad (33)$$

where the index j will represent the combined state indices $\{00, 10, 01, 11\}$. The third term can be written as

$$\mathcal{U}^\dagger H_1(t) \mathcal{U} = \mathcal{U}^\dagger \left[x f_x^{(1)}(t) + y f_y^{(1)}(t) \right] \mathcal{U}. \quad (34)$$

If we again take advantage of the parity of x, y and the ground and first excited states this simplifies to

$$\begin{aligned} \mathcal{U}^\dagger H_1(t) \mathcal{U} &= e^{-i(\omega_{10}-\omega_{00})t} f_x^{(1)} \gamma |00\rangle \langle 10| + e^{-i(\omega_{11}-\omega_{01})t} f_x^{(1)} \gamma |01\rangle \langle 11| \\ &+ e^{-i(\omega_{01}-\omega_{00})t} f_y^{(1)} \gamma |00\rangle \langle 01| + e^{-i(\omega_{11}-\omega_{10})t} f_y^{(1)} \gamma |10\rangle \langle 11| + \text{h.c.} \\ &+ \sum_j |j\rangle \langle j| H_1(t) |j\rangle \langle j|, \end{aligned} \quad (35)$$

where h.c means Hermitian conjugate and we have defined

$$\gamma = \int_{-L}^{+L} ds \Phi_0(s) s \Phi_1(s). \quad (36)$$

Then via the approximate symmetry of the unperturbed lattice (Eq. 10) we have that $\omega_{10} = \omega_{01}$, so using the fact that $\omega_d = \omega_{10} - \omega_{00}$ and $\omega_{11} = 2\omega_{10} - \omega_{00}$ we have that $\omega_{11} - \omega_{10} = \omega_d$. With these simplifications the four-level Hamiltonian can be represented by

$$H_{4L} = e^{-i\omega_d t} f_x^{(1)} \gamma |00\rangle \langle 10| + e^{-i\omega_d t} f_x^{(1)} \gamma |01\rangle \langle 11| \\ + e^{-i\omega_d t} f_y^{(1)} \gamma |00\rangle \langle 01| + e^{-i\omega_d t} f_y^{(1)} \gamma |10\rangle \langle 11| + \text{h.c.} \quad (37)$$

If we reintroduce the forms of $f_x^{(1)}$ Eq. 27 and $f_y^{(1)}$ Eq. 28 and expand each sine in terms of complex exponentials we obtain

$$H_{4L} = \frac{\hbar}{2} \left\{ \Omega_x(t) [1 + e^{-2i\omega_d t}] |00\rangle \langle 10| + \Omega_x(t) [1 + e^{-2i\omega_d t}] |01\rangle \langle 11| \right. \\ \left. + \Omega_y(t) [1 + e^{-2i\omega_d t}] |00\rangle \langle 01| + \Omega_y(t) [1 + e^{-2i\omega_d t}] |10\rangle \langle 11| \right\} + \text{h.c.} \quad (38)$$

where we have defined the couplings

$$\Omega_{x,y}(t) \equiv \frac{m\omega_d^2 \gamma g_{x,y}(t)}{\hbar}. \quad (39)$$

We now make the rotating wave approximation, in which we assume terms oscillating at $n\omega_d$ with $n \in \mathbb{Z}$ (but $n \neq 0$) average to 0 over a process of time T (ie $\omega_d \gg 1/T$). With this approximation we obtain a final four-level Hamiltonian for the shaking scheme of

$$H_{4L} = \frac{\hbar}{2} \begin{pmatrix} 0 & \Omega_x & \Omega_y & 0 \\ \Omega_x & 0 & 0 & \Omega_y \\ \Omega_y & 0 & 0 & \Omega_x \\ 0 & \Omega_y & \Omega_x & 0 \end{pmatrix}, \quad (40)$$

where we have used the ordered basis

$$|00\rangle = \begin{pmatrix} 1 \\ 0 \\ 0 \\ 0 \end{pmatrix}, \quad |10\rangle = \begin{pmatrix} 0 \\ 1 \\ 0 \\ 0 \end{pmatrix}, \quad |01\rangle = \begin{pmatrix} 0 \\ 0 \\ 1 \\ 0 \end{pmatrix}, \quad |11\rangle = \begin{pmatrix} 0 \\ 0 \\ 0 \\ 1 \end{pmatrix}. \quad (41)$$

Note the connection between this matrix representation and Fig. 4, in which the quantity Ω_x connects the basis state $|00\rangle$ to $|10\rangle$ and the state $|01\rangle$ to $|11\rangle$ (similar for Ω_y).

4.1.4 Pulse Sequences

Our goal is now to demonstrate the usefulness of the four-level approximation by deriving control schemes that bring the system to some target states. The example target states chosen here are $|\Psi_a\rangle = |01\rangle$ (ie all sites containing an atom in the first excited state in y) and

$$|\Psi_b\rangle = \frac{1}{\sqrt{2}}(|10\rangle - i|11\rangle), \quad (42)$$

which is a superposition of the first excited state in y and the first excited state in x and y . Assuming all lattice sites initially contain a single particle in the state $|00\rangle$, all atoms can be excited to the state $|\Psi_a\rangle$ via a π pulse in Ω_y . An overview of pulses is given in Appendix C. For a process of total time T , we choose $\Omega_y(t)$ to satisfy the following conditions:

- The process is smoothly turned on and off, ie $\frac{d}{dt}\Omega_y(t)$ is 0 at $t = 0$ and $t = T$,
- The control parameters are zero-valued at the start and end of the process (necessary for the final state of the system to match the target state up to some global phase, see Appendix D), ie $\Omega_y(t) = 0$ at $t = 0$ and $t = T$,
- The total pulse area is π , ie $\int_0^T \Omega_y(t) dt = \pi$.

These conditions are satisfied by the polynomial

$$\Omega_y(t) = \frac{30\pi t^2(t-T)^2}{T^5}, \quad t \in [0, T]. \quad (43)$$

If we compare this polynomial expression for $\Omega_y(t)$ with Eq. 39 we can obtain the time evolution of the control parameters that bring the system to the desired target state. In this case of lattice shaking in the y direction we have

$$Y(t) = -\frac{\hbar}{m\omega_d^2\gamma}\Omega_y(t)\cos(\omega_d t) \quad (44)$$

and $X(t) = 0$. The form of this shaking where $\Omega_y(t)$ is given by Eq. 43 is shown in Fig. 5 alongside the evolution of the state of an atom initially in $|00\rangle$. All lattice sites will evolve identically and will do so with 100% fidelity in the framework of the four-level approximation. Note that the timescale is measured in units of ω , which is the frequency of the corresponding harmonic oscillator obtained by expanding H_0 about a lattice site (see Appendix B).

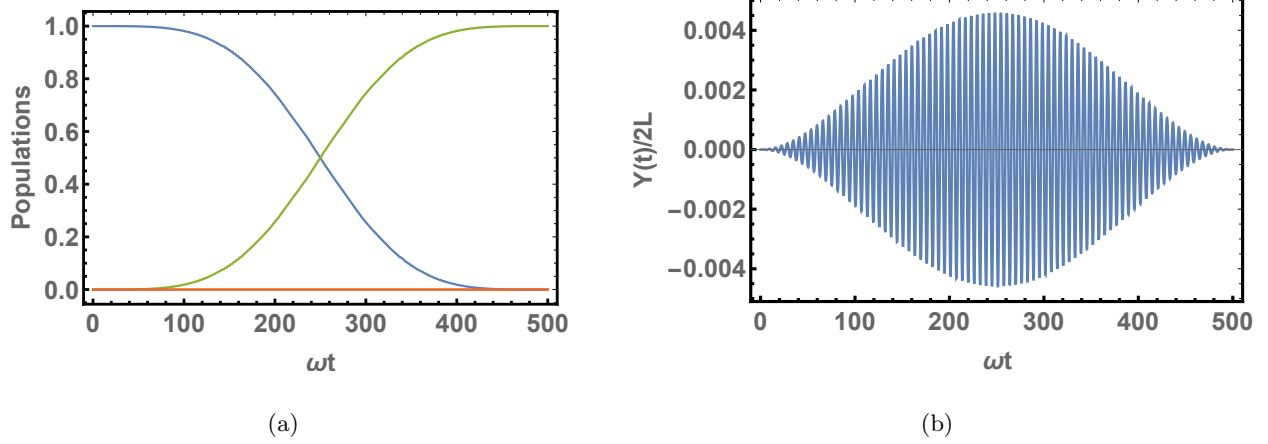


Figure 5: (a) State evolution for particle initially in state $|00\rangle$ under influence of π pulse in Ω_y . Legend: $|\langle\psi(t)|00\rangle|^2$ (blue), $|\langle\psi(t)|10\rangle|^2$ (orange), $|\langle\psi(t)|01\rangle|^2$ (green), $|\langle\psi(t)|11\rangle|^2$ (red). (b) Shaking amplitude $Y(t)$ corresponding to this π pulse represented in units of the lattice constant $2L$. Note shaking amplitudes are only a small fraction of nearest-neighbour distance.

A transfer of the population to state $|\Psi_b\rangle$ is accomplished in a piecewise manner as follows:

1. Transfer all the population to the state $|10\rangle$, which is accomplished via a π pulse in Ω_x .
2. Transfer half of the population to the state $|11\rangle$, such that an atom in a given lattice site will be in the superposition state $|\Psi_b\rangle = \frac{1}{\sqrt{2}}(|10\rangle - i|11\rangle)$. This is accomplished via a $\pi/2$ pulse in Ω_y .

For a process of total time T , we choose the first pulse to take place over a time $t_s < T$ and the second pulse over a time $T - t_s$. We choose $\Omega_x(t)$ and $\Omega_y(t)$ to satisfy similar conditions to those of $\Omega_y(t)$ in the previous section which yield the polynomial expressions

$$\Omega_x(t) = \frac{30\pi t^2(t - t_s)^2}{t_s^5}, \quad t \in [0, t_s], \quad (45)$$

$$\Omega_y(t) = \frac{15\pi(t - t_s)^2(t - T)^2}{(T - t_s)^5}, \quad t \in [t_s, T], \quad (46)$$

and are zero-valued at times other than those indicated. The state evolution resulting from this control scheme is shown for $t_s = T/2$ in Fig. 6. Note that the validity of the rotating wave approximation is discussed in Sec. 5.

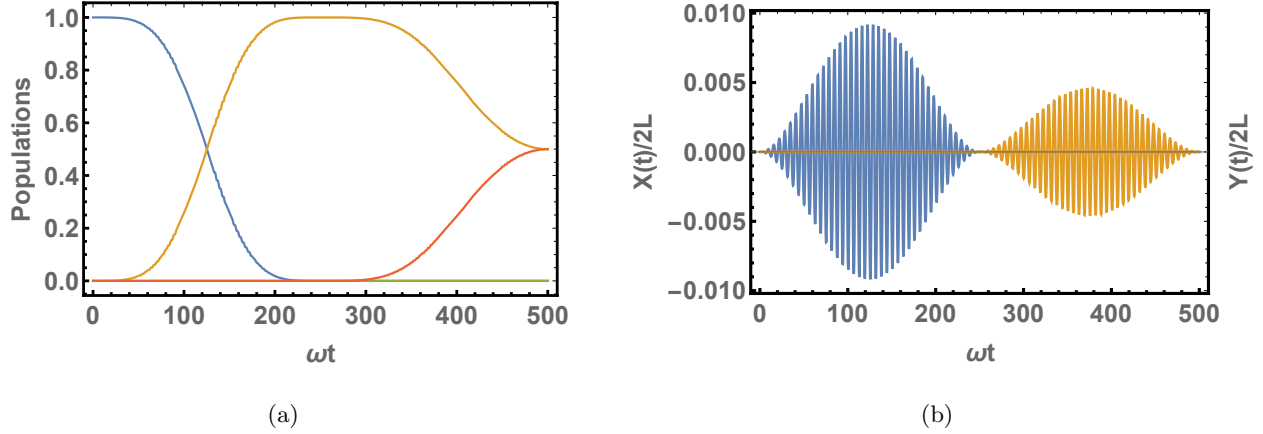


Figure 6: (a) State evolution for particle initially in state $|00\rangle$ under influence of π pulse in Ω_x followed by $\pi/2$ pulse in Ω_y . Legend: $|\langle\psi(t)|00\rangle|^2$ (blue), $|\langle\psi(t)|10\rangle|^2$ (orange), $|\langle\psi(t)|01\rangle|^2$ (green), $|\langle\psi(t)|11\rangle|^2$ (red). (b) Shaking amplitudes $X(t)$ (blue) and $Y(t)$ (orange) corresponding to this pulse sequence.

4.2 Modulation of Polarization Phase

Another method of excited state preparation is the modulation of the polarization phase between the control lasers, chosen here to be lasers 2 and 3. This method has been used in [27] to create angular momentum states in a square lattice but is here used to selectively excite lattice sites. Using the potential as in Eq. 10 and applying the same frame transformation as in the previous section we obtain the full Hamiltonian $H = H_0 + H_1(t)$ with

$$H_0 = \frac{\mathbf{p}^2}{2m} + V_0 \sin^2(\mathbf{k}_1 \cdot \mathbf{r}) + V_0 \sin^2(\mathbf{k}_2 \cdot \mathbf{r}) + V_0 \sin^2(\mathbf{k}_3 \cdot \mathbf{r}), \quad (47)$$

$$H_1(t) \equiv m\ddot{X}x + m\ddot{Y}y + V_\rho(t) \sin(\mathbf{k}_2 \cdot \mathbf{r}) \sin(\mathbf{k}_3 \cdot \mathbf{r}). \quad (48)$$

As before we define the functions $f_x^{(2)}(t) = m\ddot{X}$ and $f_y^{(2)}(t) = m\ddot{Y}$, but here we assume these functions to be slow varying compared to ω_d in contrast to the previous section.

4.2.1 Four-level Approximation

We again assume the system can be described by the states $|00\rangle$, $|10\rangle$, $|01\rangle$, and $|11\rangle$ and apply the unitary transformation \mathcal{U} as defined by Eq. 30 to obtain the four-level Hamiltonian

$$\begin{aligned} H_{4L} = & e^{-i\omega_d t} \mathcal{X}_{00}^* \mathcal{X}_{10} f_x^{(2)} \gamma |00\rangle \langle 10| + e^{-i\omega_d t} \mathcal{X}_{01}^* \mathcal{X}_{11} f_x^{(2)} \gamma |01\rangle \langle 11| \\ & + e^{-i\omega_d t} \mathcal{X}_{00}^* \mathcal{X}_{01} f_y^{(2)} \gamma |00\rangle \langle 01| + e^{-i\omega_d t} \mathcal{X}_{10}^* \mathcal{X}_{11} f_y^{(2)} \gamma |10\rangle \langle 11| + \text{h.c.} \end{aligned} \quad (49)$$

where a $*$ represents a complex conjugate. We can also expand the $\mathcal{X}_{ab}^* \mathcal{X}_{cd}$ terms by exploiting the parity properties of the basis states, such that all overlaps with odd terms (ie x and y) are zero and we can write

$$\langle nm | H_1(s) | nm \rangle = V_\rho(t)(\alpha_n + \beta_m - 1) \quad (50)$$

where we have defined

$$\alpha_n = \int_{-L}^{+L} ds \Phi_n(s) \cos^2\left(\frac{\sqrt{3}}{2}ks\right) \Phi_n(s), \quad (51)$$

$$\beta_n = \int_{-L}^{+L} ds \Phi_n(s) \cos^2\left(\frac{1}{2}ks\right) \Phi_n(s). \quad (52)$$

Thus the $\mathcal{X}_{ab}^* \mathcal{X}_{cd}$ terms can be written as

$$\mathcal{X}_{ab}^* \mathcal{X}_{cd} = \exp\left[\frac{i}{\hbar}(\alpha_a + \beta_b - \alpha_c - \beta_d) \int_0^t ds V_\rho(s)\right], \quad (53)$$

and the four-level Hamiltonian simplifies to

$$\begin{aligned} H_{4L} = & \gamma e^{-i\omega_d t} f_x^{(2)}(t) \exp\left[\frac{i}{\hbar}(\alpha_0 - \alpha_1) \int_0^t ds V_\rho(s)\right] |00\rangle \langle 10| \\ & + \gamma e^{-i\omega_d t} f_x^{(2)}(t) \exp\left[\frac{i}{\hbar}(\alpha_0 - \alpha_1) \int_0^t ds V_\rho(s)\right] |01\rangle \langle 11| \\ & + \gamma e^{-i\omega_d t} f_y^{(2)}(t) \exp\left[\frac{i}{\hbar}(\beta_0 - \beta_1) \int_0^t ds V_\rho(s)\right] |00\rangle \langle 01| \\ & + \gamma e^{-i\omega_d t} f_y^{(2)}(t) \exp\left[\frac{i}{\hbar}(\beta_0 - \beta_1) \int_0^t ds V_\rho(s)\right] |10\rangle \langle 11| + \text{h.c.} \end{aligned} \quad (54)$$

4.2.2 Selective Site excitation

We now examine the effect of the interference term $V_\rho(t) \sin(\mathbf{k}_2 \cdot \mathbf{r}) \sin(\mathbf{k}_3 \cdot \mathbf{r})$ at different lattice sites. If we write the spatial part of this interference $I(\mathbf{r}) \equiv \sin(\mathbf{k}_2 \cdot \mathbf{r}) \sin(\mathbf{k}_3 \cdot \mathbf{r})$ in terms of x and y we obtain

$$I(\mathbf{r}) = \frac{1}{2} \left[\cos(\sqrt{3}kx) - \cos(ky) \right], \quad (55)$$

where $\mathbf{r} = (x, y)$. If we displace the coordinates by n lattice sites along the \mathbf{k}_1^\perp direction, using the nearest neighbour spacing $2L = 2\pi/\sqrt{3}k$ and the forms of the \mathbf{k}_j^\perp Eq. 11 then I changes as

$$I(\mathbf{r} - n(2L)\hat{\mathbf{k}}_1^\perp) = \frac{1}{2} \left[\cos(\sqrt{3}kx + 2n\pi) - \cos(ky) \right] = I(\mathbf{r}), \quad (56)$$

ie the effect of the interference term is identical at all lattice sites along the \mathbf{k}_1^\perp direction (which happens to be $-\hat{\mathbf{x}}$). If we then perform the same calculation for displacements along the \mathbf{k}_2^\perp and

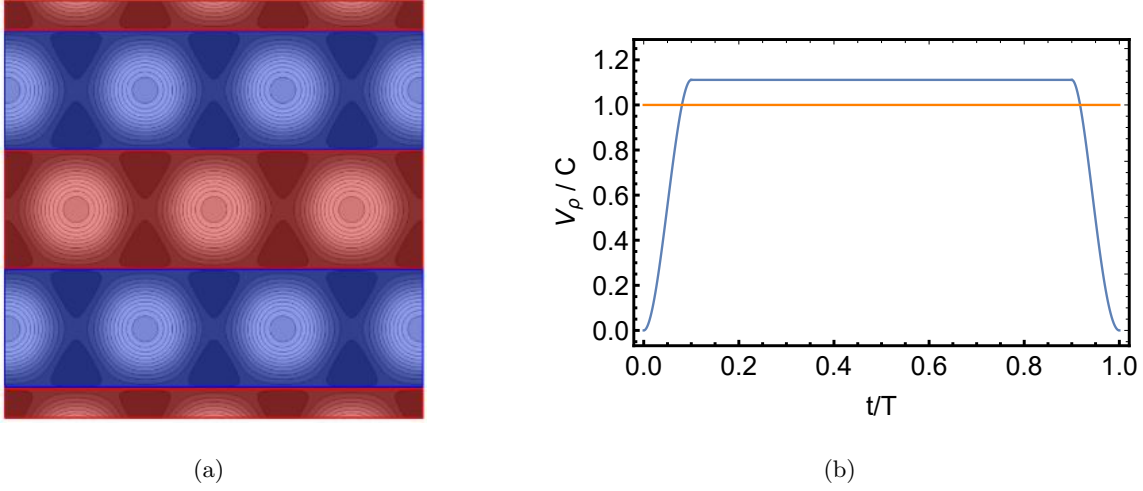


Figure 7: (a) Change in sign of interference term at different bands of lattice sites (if interference term is positive along red bands then it is negative along blue) (b) $V_\rho(t)$ with ramp-up time $\tau = T/10$.

\mathbf{k}_3^\perp directions we obtain

$$I(\mathbf{r} - n(2L)\hat{\mathbf{k}}_2^\perp) = \frac{1}{2} \left[\cos(\sqrt{3}kx - n\pi) - \cos(ky - n\pi) \right] = (-1)^n I(\mathbf{r}), \quad (57)$$

$$I(\mathbf{r} - n(2L)\hat{\mathbf{k}}_3^\perp) = \frac{1}{2} \left[\cos(\sqrt{3}kx - n\pi) - \cos(ky + n\pi) \right] = (-1)^n I(\mathbf{r}). \quad (58)$$

These relations⁶ imply that the interference term changes sign along bands of sites which have the same x coordinate as in Fig. 7. We can therefore choose $V_\rho(t)$ such that along a given band and each band $2\pi/k$ displaced from this band in $\hat{\mathbf{y}}$ we have

$$\mathcal{X}_{ab}^* \mathcal{X}_{cd} \simeq e^{i\omega_d t}, \quad (59)$$

while on all bands in between we have

$$\mathcal{X}_{ab}^* \mathcal{X}_{cd} \simeq -e^{i\omega_d t}. \quad (60)$$

This is equivalent to requiring that for excitations in x ,

$$\int_0^t ds V_\rho(s) \simeq \frac{\hbar\omega_d t}{\alpha_0 - \alpha_1}, \quad (61)$$

while for excitations in y

$$\int_0^t ds V_\rho(s) \simeq \frac{\hbar\omega_d t}{\beta_0 - \beta_1}. \quad (62)$$

⁶Note that the third relation is superfluous, as the three \mathbf{k}_j^\perp are not linearly independent. A displacement along \mathbf{k}_3^\perp can be described by a displacement along $-\mathbf{k}_2^\perp$ and then along $-\mathbf{k}_1^\perp$. Since $I(\mathbf{r})$ is invariant under displacements along \mathbf{k}_1^\perp , then I must change along \mathbf{k}_3^\perp as it does along \mathbf{k}_2^\perp .

At all sites where $\mathcal{X}_{ab}^* \mathcal{X}_{cd} \simeq e^{i\omega_d t}$, all terms in H_{4L} will be proportional to $e^{\pm 2i\omega_d t}$ and thus the rotating wave approximation can be applied, such that the Hamiltonian has no effect at these sites. At all sites where $\mathcal{X}_{ab}^* \mathcal{X}_{cd} \simeq e^{-i\omega_d t}$, all terms in H_{4L} will be proportional to $e^0 = 1$, and the Hamiltonian reduces to that of the previous section Eq. 40 (but with $\Omega_{x,y}(t) = 2\gamma f_{x,y}^{(2)}(t)/\hbar$). Therefore we can selectively excite bands of atoms via pulses in Ω_x and Ω_y provided we manipulate V_ρ in an appropriate manner.

If $V_\rho(t)$ is chosen to be a smoothed tophat function as in Fig. 7, then the Hamiltonian will only act on alternating bands of sites. This effect is shown for both a lattice site where the Hamiltonian is turned “on” and where the Hamiltonian is turned “off” in Fig. 8, where the initial state is $|00\rangle$, the target state is $|10\rangle$ and as usual we accomplish this via a π pulse in Ω_x . To minimise error in the approximation it is useful to choose the peak value of ρ to be slightly higher than the value it must “match” denoted C (for example $C = \hbar\omega_d/(\alpha_0 - \alpha_1)$ in the case of a pulse in x), where the discrepancy depends on the ramp-up and ramp-down time τ . For given τ we choose a peak value for the smoothed tophat function of

$$V_{\rho,max} = \frac{CT}{T - \tau}, \quad (63)$$

or in terms of the parameter $\tau' = \tau/T$, which is the ramp-up time as a proportion of the total process time T

$$V_{\rho,max} = \frac{C}{1 - \tau'}. \quad (64)$$

With this choice of V_ρ we expect an error of $\mathcal{O}(\tau)$ in the approximation such that at any time t we have

$$\frac{\alpha_0 - \alpha_1}{\hbar} \int_0^t ds V_\rho(s) = \omega_d t + \mathcal{O}(\tau). \quad (65)$$

Therefore the validity of applying the rotating wave approximation here depends linearly on the ramp-up time, which is assumed to be equal to the ramp-down time.

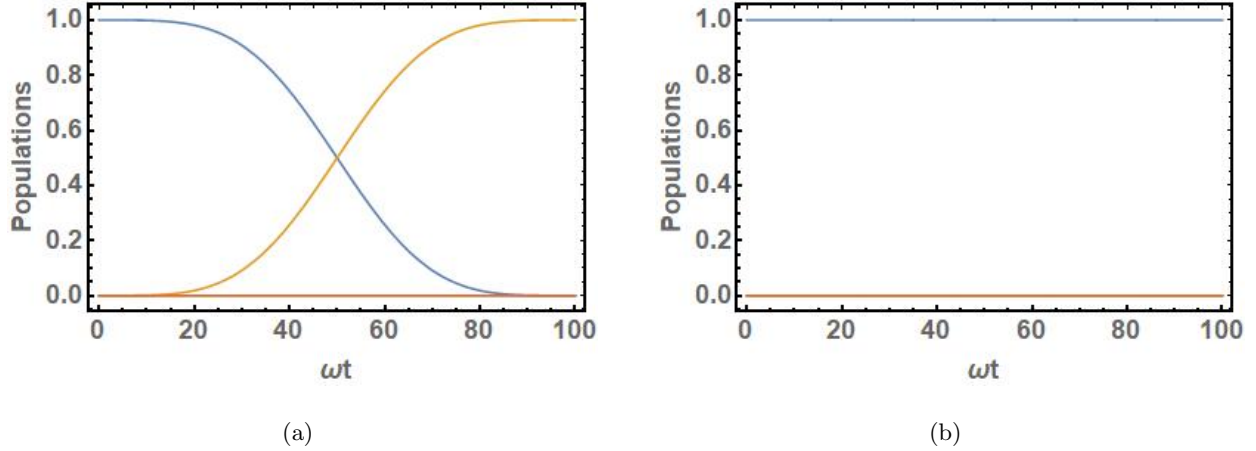


Figure 8: (a) State evolution for particle initially in state $|00\rangle$ under influence of π pulse in Ω_x . Legend: $|\langle\psi(t)|00\rangle|^2$ (blue), $|\langle\psi(t)|10\rangle|^2$ (orange), $|\langle\psi(t)|01\rangle|^2$ (green), $|\langle\psi(t)|11\rangle|^2$ (red). (b) State evolution on lattice site where interference term is effectively “turned off” via interference term modulation.

4.3 Amplitude Modulation

The final method of generating excited states in an optical lattice developed in this report is the modulation of the control laser amplitude. Here we establish a control scheme for amplitude modulation in a triangular lattice with the goal of creating a large angular momentum state, in which each lattice site is occupied by an atom in the superposition

$$|+\rangle = \frac{1}{\sqrt{2}}(|20\rangle + i|02\rangle), \quad (66)$$

which is an eigenstate of the z component of the angular momentum operator L_z , such that $L_z|+\rangle \simeq 2\hbar|+\rangle$. Transitioning a lattice of atoms in the ground state $|00\rangle$ to this state $|+\rangle$ via amplitude modulation was already investigated in [27] using a square lattice and a second square lattice rotated relative to the first, but here we create this large angular momentum state in a triangular lattice geometry.

4.3.1 Alternative Lattice Potential

We now use a lattice potential slightly different to that of the previous sections, as now we no longer have control parameters $\phi_j(t)$ and $\rho(t)$ but instead $A_1(t)$ related to the amplitude of laser 1 and

$A_{2,3}(t)$, related to the common amplitude of lasers 2 and 3. We choose to write the electric field as

$$\begin{aligned}\mathbf{E}(\mathbf{r}, t) = & \mathbf{E}_0 \sqrt{1 + A_1(t)} e^{-i(\omega+\epsilon)t} \sin(\mathbf{k}_1 \cdot \mathbf{r}) \\ & + \mathbf{E}_0 \sqrt{1 + A_{2,3}(t)} e^{-i\omega t} \sin(\mathbf{k}_2 \cdot \mathbf{r}) \\ & + \mathbf{E}_0 e^{-i\theta} \sqrt{1 + A_{2,3}(t)} e^{-i\omega t} \sin(\mathbf{k}_3 \cdot \mathbf{r})\end{aligned}\quad (67)$$

where we have assumed the frequency of laser 1 is detuned by an amount ϵ as in Sec. 3.1 and θ represents the time-independent polarization phase difference between lasers 2 and 3. Calculating the potential structure according to Eq. 3 and assuming terms oscillating at ϵ can be neglected we obtain

$$\begin{aligned}V(\mathbf{r}, t) = & V_0 [1 + A_1(t)] \sin^2(\mathbf{k}_1 \cdot \mathbf{r}) + V_0 [1 + A_{2,3}(t)] \sin^2(\mathbf{k}_2 \cdot \mathbf{r}) \\ & + V_0 [1 + A_{2,3}(t)] \sin^2(\mathbf{k}_3 \cdot \mathbf{r}) + 2V_0 [1 + A_{2,3}(t)] \cos(\theta) \sin(\mathbf{k}_2 \cdot \mathbf{r}) \sin(\mathbf{k}_3 \cdot \mathbf{r}).\end{aligned}\quad (68)$$

If we then assume lasers 2 and 3 are orthogonally polarised (ie $\theta = \pi/2$) and define $a(t) \equiv V_0 A_1(t)$ and $b(t) \equiv V_0 A_{2,3}(t)$ then we can write down the Hamiltonian of the system in the lab frame $H(t) = H_0 + H_1(t)$ with

$$H_0 = \frac{\mathbf{p}^2}{2m} + V_0 \sin^2(\mathbf{k}_1 \cdot \mathbf{r}) + V_0 \sin^2(\mathbf{k}_2 \cdot \mathbf{r}) + V_0 \sin^2(\mathbf{k}_3 \cdot \mathbf{r}),\quad (69)$$

$$H_1(t) \equiv a(t) \sin^2(\mathbf{k}_1 \cdot \mathbf{r}) + b(t) [\sin^2(\mathbf{k}_2 \cdot \mathbf{r}) + \sin^2(\mathbf{k}_3 \cdot \mathbf{r})].\quad (70)$$

Using the forms of the \mathbf{k}_j as in Eq. 2 we can rewrite $H_1(t)$ as

$$H_1(t) = a(t) \sin^2(ky) - b(t) \cos(\sqrt{3}kx) \cos(ky) + b(t)\quad (71)$$

The time-dependent energy shift $b(t)$ to the Hamiltonian can be disregarded, as in a similar manner to Eq. 20 we can define a unitary transformation

$$\mathcal{V} \equiv \exp\left(-\frac{i}{\hbar} \int_0^t ds b(s)\right)\quad (72)$$

which commutes with the Hamiltonian, so that under this transformation H_0 remains unchanged and $H_1(t)$ becomes

$$H_1(t) = a(t) \sin^2(ky) - b(t) \cos(\sqrt{3}kx) \cos(ky).\quad (73)$$

4.3.2 Four-level Approximation

We now approximate the dynamics of the system as being described by the basis of states of eigenstates of H_0 : $\{|00\rangle, |20\rangle, |02\rangle, |22\rangle\}$, i.e. we consider only excitations to second excited states in x and y . This level scheme is shown in Fig. 9. We choose these four basis states as they are resonantly coupled and we choose control parameters which excite on-resonance with the $|00\rangle$ to $|20\rangle$ or $|02\rangle$ transition. As before the anharmonicity of the potential detunes higher energy states and thus these states can be neglected. Again we utilize the unitary transformation \mathcal{U} as defined by Eq. 30 to remove the diagonal elements of \tilde{H}_{4L} (the matrix representation of the particle Hamiltonian in this basis), in order to examine the couplings between different basis states. Evaluating $\tilde{H}_{4L}(t) = \mathcal{U}^\dagger H \mathcal{U} - i\hbar \mathcal{U}^\dagger \dot{\mathcal{U}}$ we obtain

$$\begin{aligned}
\tilde{H}_{4L} = & e^{i(\omega_{20}-\omega_{00})t} \mathcal{X}_{00}^* \mathcal{X}_{20} \langle 00| H_1(t) |20\rangle |00\rangle \langle 20| \\
& + e^{i(\omega_{02}-\omega_{00})t} \mathcal{X}_{00}^* \mathcal{X}_{02} \langle 00| H_1(t) |02\rangle |00\rangle \langle 02| \\
& + e^{i(\omega_{22}-\omega_{00})t} \mathcal{X}_{00}^* \mathcal{X}_{22} \langle 00| H_1(t) |22\rangle |00\rangle \langle 22| \\
& + e^{i(\omega_{02}-\omega_{20})t} \mathcal{X}_{20}^* \mathcal{X}_{02} \langle 20| H_1(t) |02\rangle |20\rangle \langle 02| \\
& + e^{i(\omega_{22}-\omega_{20})t} \mathcal{X}_{20}^* \mathcal{X}_{22} \langle 20| H_1(t) |22\rangle |20\rangle \langle 22| \\
& + e^{i(\omega_{22}-\omega_{02})t} \mathcal{X}_{02}^* \mathcal{X}_{22} \langle 02| H_1(t) |22\rangle |02\rangle \langle 22| + \text{h.c.}
\end{aligned} \tag{74}$$

We then make several simplifications to the form of \tilde{H}_{4L} , the first of which by noting that due to the approximate symmetry of the unperturbed lattice we have $\omega_{20} = \omega_{02}$, and so with $\tilde{\omega}_d \equiv \omega_{20} - \omega_{00}$ we note that $\omega_{22} - \omega_{00} = 2\tilde{\omega}_d$.

The second simplification is to expand the $\langle nm| H_1(t) |pq\rangle$ terms; if we define

$$C_{ij}(\eta) \equiv \int_{-L}^{+L} ds \Phi_i(s) \cos(\eta ks) \Phi_j(s) = C_{ji}(\eta), \tag{75}$$

$$S_{ij} \equiv \int_{-L}^{+L} ds \Phi_i(s) \sin^2(ks) \Phi_j(s) = S_{ji}, \tag{76}$$

then we can write

$$\langle nm| H_1(t) |pq\rangle = a(t) S_{mq} \delta_{np} - b(t) C_{np}(\sqrt{3}) C_{mq}(1), \tag{77}$$

where δ_{np} is the Kronecker delta for indices n, p . Finally we simplify the $\mathcal{X}_{nm} \mathcal{X}_{pq}$ terms, which can

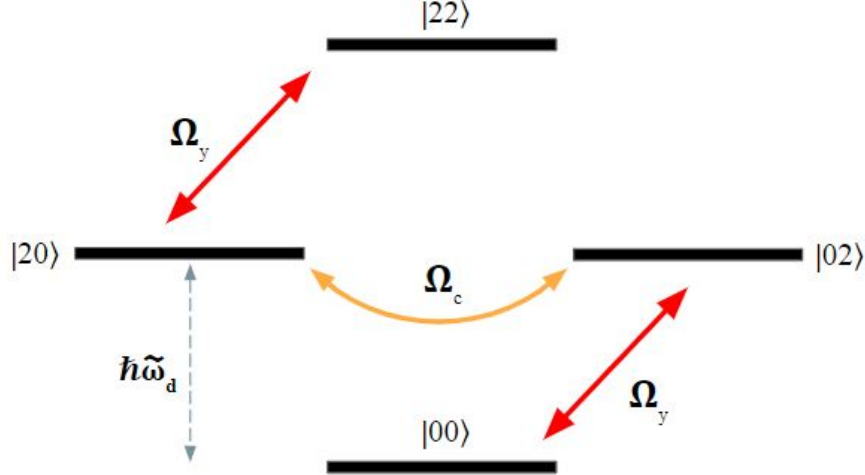


Figure 9: Four-level scheme of second excited states and the coupling parameters between them.

be written explicitly as

$$\mathcal{X}_{nm}^*(t)\mathcal{X}_{pq}(t) = \exp\left[\frac{i}{\hbar}\int_0^t ds \langle nm|H_1(s)|nm\rangle - \frac{i}{\hbar}\int_0^t ds \langle pq|H_1(s)|pq\rangle\right]. \quad (78)$$

Then using the previous simplification we may write this as

$$\mathcal{X}_{nm}^*(t)\mathcal{X}_{pq}(t) = \exp\left[\frac{i}{\hbar}(S_{mm} - S_{qq})\int_0^t ds a(s)\right]G_{nmpq}(t), \quad (79)$$

where we have defined

$$G_{nmpq}(t) \equiv \exp\left\{\frac{i}{\hbar}\left[C_{pp}(\sqrt{3})C_{qq}(1) - C_{nn}(\sqrt{3})C_{mm}(1)\right]\int_0^t ds b(s)\right\}. \quad (80)$$

Let us now assume a particular form of the amplitude modulation of laser 1

$$a(t) = g(t)\cos(\tilde{\omega}_d t), \quad (81)$$

which is on-resonance with the transition from $|00\rangle$ to $|20\rangle$, with a slowly varying envelope $g(t)$.

With this form of amplitude modulation we can make the approximation

$$\begin{aligned} \int_0^t ds a(s) &= \int_0^t ds g(s)\cos(\tilde{\omega}_d s) \\ &= \frac{1}{\tilde{\omega}_d}\left[g(t)\sin(\tilde{\omega}_d t) - \int_0^t \dot{g}(s)\sin(\tilde{\omega}_d s) ds\right] \\ &\simeq \frac{1}{\tilde{\omega}_d}g(t)\sin(\tilde{\omega}_d t), \end{aligned} \quad (82)$$

where in the final step we assume $\dot{g} \simeq 0$. With this approximation we can write the $\mathcal{X}_{nm}^*\mathcal{X}_{pq}$ as

$$\mathcal{X}_{nm}^*(t)\mathcal{X}_{pq}(t) \simeq \exp[-ig(t)A_{qm}\sin(\tilde{\omega}_d t)]G_{nmpq}(t), \quad (83)$$

where we have defined

$$A_{mq} \equiv \frac{S_{qq} - S_{mm}}{\hbar\tilde{\omega}_d}. \quad (84)$$

We then make use of the Jacobi-Anger expansion [28]

$$e^{-i\kappa \sin(\lambda t)} = \sum_{k=-\infty}^{+\infty} J_k(\kappa) e^{-ik\lambda t}, \quad (85)$$

where $J_k(\kappa)$ is the k^{th} Bessel function of the first kind, to write

$$\mathcal{X}_{nm}^*(t)\mathcal{X}_{pq}(t) = G_{nmpq}(t) \sum_{k=-\infty}^{+\infty} J_k[g(t)A_{mq}] e^{-ik\tilde{\omega}_d t}. \quad (86)$$

There are two kinds of terms in \tilde{H}_{4L} , the first of which is

$$e^{\pm i\tilde{\omega}_d t} a(t) S_{02} \mathcal{X}_{ab}^* \mathcal{X}_{ac}. \quad (87)$$

Let us simplify these terms by first writing $a(t)$ Eq. 81 in terms of complex exponentials and expanding the $\mathcal{X}_{ab}^* \mathcal{X}_{ac}$ via Eq. 83. This yields

$$= \frac{g(t)S_{02}}{2} (1 + e^{\pm 2i\tilde{\omega}_d t}) G_{abac}(t) \sum_{k=-\infty}^{+\infty} J_k[g(t)A_{bc}] e^{-ik\tilde{\omega}_d t}. \quad (88)$$

We then make the rotating wave approximation, whereby all terms oscillating at $n\tilde{\omega}_d$ with $n \in \mathbb{Z}$ (but $n \neq 0$) average to 0, such that we retain only the terms

$$\simeq \frac{g(t)S_{02}}{2} G_{abad}(t) \{J_0[g(t)A_{bc}] + J_{\pm 2}[g(t)A_{bc}]\}. \quad (89)$$

Note that the $G_{abac}(t)$ term survives the rotating wave approximation, as the term $C_{pp}(\sqrt{3})C_{qq}(1) - C_{nn}(\sqrt{3})C_{mm}(1) \ll \tilde{\omega}_d/\omega$ for a typical well depth of $3V_0/\hbar\omega$. The validity of this statement is confirmed via numerical calculation of the overlap integrals in Fig. 10 (b), where it is assumed that the eigenstates are that of the 2D harmonic oscillator. We then note that $A_{00} = A_{22} = 0$ and $A_{02} \ll 1$ as is also shown in Fig. 10 (b), and therefore we make the approximations $J_0[g(t)A_{bc}] \simeq 1$ and $J_{1,2}[g(t)A_{bc}] \simeq 0$ to obtain

$$e^{\pm i\tilde{\omega}_d t} a(t) S_{02} \mathcal{X}_{ab}^* \mathcal{X}_{ac} \simeq \frac{g(t)S_{02}}{2} G_{abad}(t). \quad (90)$$

If we impose that we always perform modulation pulses in a piecewise manner (ie if $a(t) \neq 0$ then $b(t) = 0$ and vice versa) then we have the final form of the first type of term

$$e^{\pm i\tilde{\omega}_d t} a(t) S_{02} \mathcal{X}_{ab}^* \mathcal{X}_{ac} \simeq \frac{g(t)S_{02}}{2}. \quad (91)$$

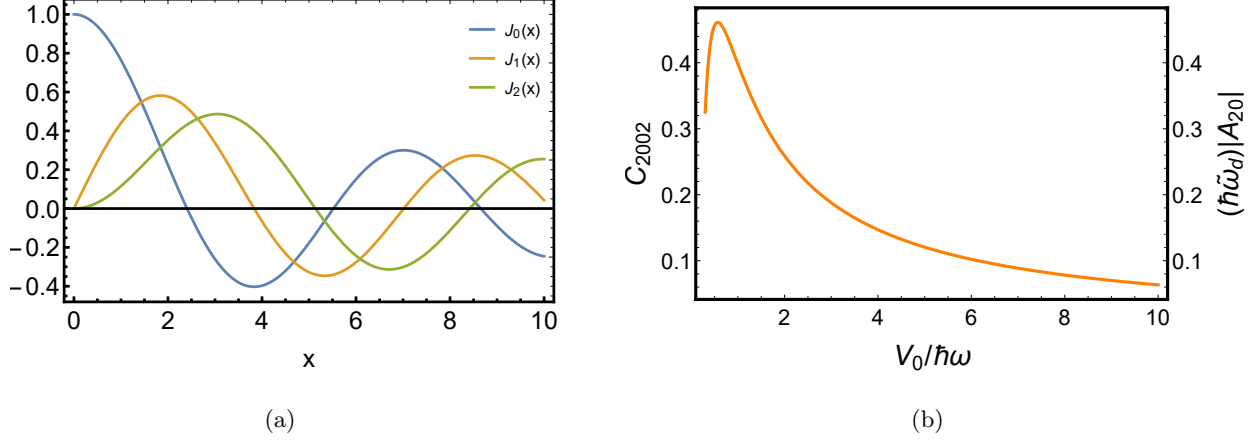


Figure 10: (a) Bessel functions of the first kind. (b) Parameters A_{mq} and $C_{2002} \equiv C_{00}(\sqrt{3})C_{22}(1) - C_{22}(\sqrt{3})C_{00}(1)$ as a function of lattice depth. Note the coincidental identical evolution of both parameters.

Now we examine the second type of term, which is of the form

$$e^{\pm Ni\tilde{\omega}at} b(t) C_{ac}(\sqrt{3}) C_{bd}(1) \mathcal{X}_{ab}^* \mathcal{X}_{cd}, \quad N \in \{0, 1, 2\}. \quad (92)$$

By again using the Jacobi-Anger expansion of the $\mathcal{X}_{ab}^* \mathcal{X}_{cd}$ we obtain

$$= b(t) C_{ac}(\sqrt{3}) C_{bd}(1) e^{\pm Ni\tilde{\omega}at} \left\{ G_{abcd}(t) \sum_{k=-\infty}^{+\infty} J_k[g(t) A_{qm}] e^{-ik\tilde{\omega}at} \right\}. \quad (93)$$

If we again make the rotating wave approximation we are left with a single term for a given N :

$$\simeq b(t) C_{ac}(\sqrt{3}) C_{bd}(1) G_{abcd}(t) J_{\pm N}[g(t) A_{qm}]. \quad (94)$$

As before we make the approximations $J_0[g(t) A_{qm}] \simeq 1$ and $J_{1,2}[g(t) A_{qm}] \simeq 0$ and note that for integer n , $J_{-n} = (-1)^n J_n$ to obtain

$$\simeq \begin{cases} b(t) C_{ac}(\sqrt{3}) C_{bd}(1) G_{abcd}(t) & \text{for } N = 0 \\ 0 & \text{for } N = \pm 1, \pm 2 \end{cases} \quad (95)$$

For convenience we assume that the term $G_{2002} \simeq 1$ (which is accurate for typical well depths of $\sim 3V_0/\hbar\omega$ as $C_{00}(\sqrt{3})C_{22}(1) - C_{22}(\sqrt{3})C_{00}(1) \sim 0.1$) but note that this is not a strict assumption as the dynamics can still be obtained relatively easily by numerical means. With all these simplifications we may return to the four-level Hamiltonian Eq. 74 which can now be written as

$$\tilde{H}_{4L} \simeq \frac{\hbar}{2} \left\{ \Omega_c(t) |20\rangle \langle 02| + \Omega_y(t) |00\rangle \langle 02| + \Omega_y(t) |20\rangle \langle 22| \right\} + \text{h.c.} \quad (96)$$

where we have defined the couplings

$$\Omega_y(t) = -\frac{g(t)S_{02}}{\hbar}, \quad (97)$$

$$\Omega_c(t) = \frac{2b(t)C_{20}(\sqrt{3})C_{02}(1)}{\hbar}. \quad (98)$$

This can be represented in matrix form as

$$\tilde{H}_{4L} = \frac{\hbar}{2} \begin{pmatrix} 0 & 0 & \Omega_y & 0 \\ 0 & 0 & \Omega_c & \Omega_y \\ \Omega_y & \Omega_c & 0 & 0 \\ 0 & \Omega_y & 0 & 0 \end{pmatrix}, \quad (99)$$

where we have used the ordered basis

$$|00\rangle = \begin{pmatrix} 1 \\ 0 \\ 0 \\ 0 \end{pmatrix}, \quad |20\rangle = \begin{pmatrix} 0 \\ 1 \\ 0 \\ 0 \end{pmatrix}, \quad |02\rangle = \begin{pmatrix} 0 \\ 0 \\ 1 \\ 0 \end{pmatrix}, \quad |22\rangle = \begin{pmatrix} 0 \\ 0 \\ 0 \\ 1 \end{pmatrix}. \quad (100)$$

Again note the connection between this matrix representation and the energy level diagram Fig. 9, wherein Ω_y connects the state $|00\rangle$ to $|02\rangle$ and the state $|20\rangle$ to $|22\rangle$, while the quantity Ω_c couples $|02\rangle$ to $|20\rangle$.

4.3.3 Control Scheme

We now seek the control scheme that takes our atoms to the state $|+\rangle = \frac{1}{\sqrt{2}}(|20\rangle + i|02\rangle)$, which is an angular-momentum state with angular momentum $\simeq 2\hbar$. As before we accomplish this in the four-level scheme via a piecewise process:

1. Transfer all the population to the state $|02\rangle$, which is accomplished via a π pulse in Ω_y .
2. Transfer half of the population to the state $|20\rangle$, such that an atom in a given lattice site will be in the superposition state $|\Psi\rangle = \frac{1}{\sqrt{2}}(|20\rangle + i|02\rangle)$. This is accomplished via a $-\pi/2$ pulse in Ω_c .

For a process of total time T , we choose the first pulse to take place over a time $t_s < T$ and the second pulse over a time $T - t_s$. As in previous sections we choose $\Omega_y(t)$ and $\Omega_c(t)$ to be smooth

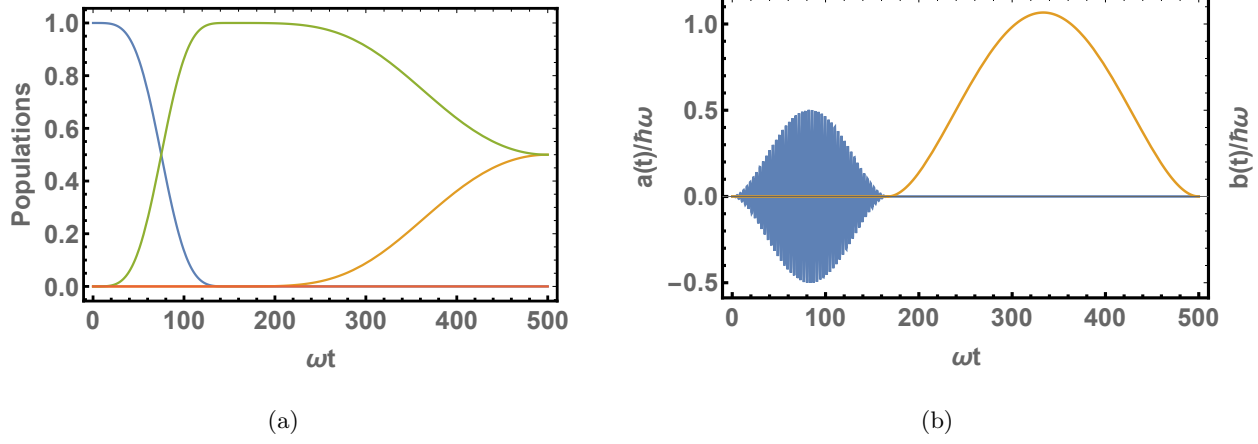


Figure 11: (a) State evolution for particle initially in state $|00\rangle$ under influence of π pulse in Ω_y of duration $t_s = T/3$ and a $-\pi/2$ pulse in Ω_c to achieve target state $|+\rangle$. Legend: $|\langle\psi(t)|00\rangle|^2$ (blue), $|\langle\psi(t)|20\rangle|^2$ (orange), $|\langle\psi(t)|02\rangle|^2$ (green), $|\langle\psi(t)|22\rangle|^2$ (red). (b) Amplitude modulation $a(t)$ (blue) and $b(t)$ (orange) corresponding to this control sequence.

varying functions that are zero-valued at the endpoints of the pulses such that

$$\Omega_y(t) = \frac{30\pi t^2(t-t_s)^2}{t_s^5}, \quad t \in [0, t_s], \quad (101)$$

$$\Omega_c(t) = \frac{15\pi(t-t_s)^2(t-T)^2}{(T-t_s)^5}, \quad t \in [t_s, T], \quad (102)$$

and are zero-valued at times other than those indicated. If we write the control parameters in terms of the couplings $\Omega_{y,c}(t)$ we obtain

$$a(t) = -\frac{\hbar}{S_{02}}\Omega_y(t)\cos(\tilde{\omega}_d t), \quad (103)$$

$$b(t) = \frac{\hbar}{2C_{20}(\sqrt{3})C_{02}(1)}\Omega_c(t). \quad (104)$$

The evolution of the state of an atom in a given lattice site under these control parameters is shown in Fig. 11 for $t_s = T/3$ and a total time $T = 500\omega$, where as in previous sections ω is the harmonic frequency of the lattice site with $\omega^2 = 3V_0k^2/m$.

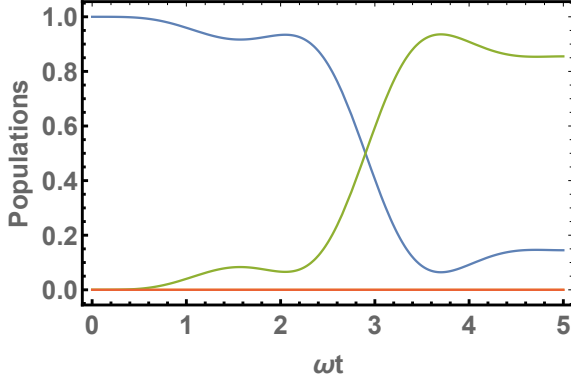
5 Discussion

There are two primary assumptions made in the derivation of the previous 4-level schemes, namely (i) the rotating wave approximation is valid and (ii) the dynamics of the system are accurately described by a four state basis. The first of these assumptions is easily investigated and understood. Fig. 12 depicts the evolution of the state of an atom in a given lattice site under both of the control schemes designed in Sec. 4.1 for varying total process times T . For $T = 5\omega$ and $T = 10\omega$ the rotating wave approximation has begun to break down, and as a result the fidelity of the final state is reduced. The degradation in fidelity⁷ with decreasing T is shown in Fig. 13 for the shaking process derived in Sec. 4.1.4 which excites atoms from the ground state $|00\rangle$ to the state $|\Psi_b\rangle$.

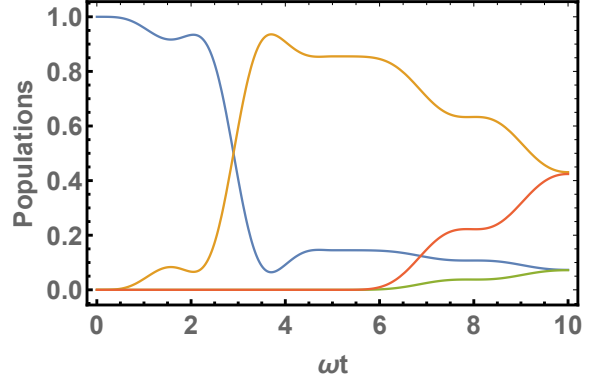
Note that in the piecewise scheme of Sec. 4.1.4 it has been assumed that $t_s = T/2$, ie that both pulses take place over half the total process time. This is the optimal choice for this scheme as both pulses rely on the rotating wave approximation. For example if t_s were chosen to be $T/10$, the pulse taking place over $9T/10$ would have relatively high fidelity, but the shorter pulse would be relatively inaccurate. To ensure the validity of the rotating wave approximation and the slow varying shaking amplitude envelope assumption that $\dot{g}(t) \simeq 0$ we simply need to impose the heuristic condition $T \gg (\omega_d)^{-1} \simeq (\omega)^{-1}$ as in [29] where $\omega^2 = 3V_0k^2/m$ is the approximate harmonic oscillator frequency at each lattice site. In the case of excitations to the second excited state this condition becomes $T \gg (\tilde{\omega}_d)^{-1} \simeq (2\omega)^{-1}$.

In the harmonic limit the energy levels become equally spaced (energies of the quantum harmonic oscillator are $\hbar\omega(n + 1/2)$, $n \in \mathbb{N}_0$) and therefore higher levels become resonantly coupled. In this regime further energy levels are required in the basis to fully describe the system (see Appendix B of [29] where a 6-level approximation is developed for the deep-well limit). For example, if the system were described exactly by a harmonic oscillator in x and y (ie $\omega_d \rightarrow \omega$ and $\tilde{\omega}_d \rightarrow 2\omega$) then shaking in x on resonance with the $|00\rangle$ to $|10\rangle$ transition would resonantly couple the state $|20\rangle$ which would then need to be included in the basis of states. In the 4-level model shaking on-resonance with the desired transition gives the best results but a small detuning in shaking frequency actually reduces leakage to higher levels by detuning levels not included in the 4-level model. In this anharmonic case the resonance curve is slightly shifted such that by slightly increasing the detuning of Ω_x or

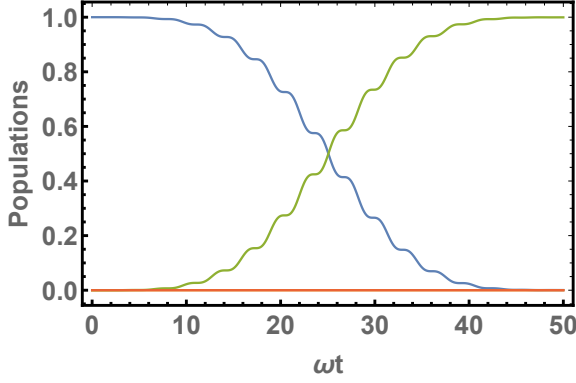
⁷The term ‘‘fidelity’’ refers to the accuracy of the final state, in that if our target state is $|\Psi\rangle$, then the fidelity of our state $\psi(t)$ at a time T is $|\langle\Psi|\psi(T)\rangle|^2$



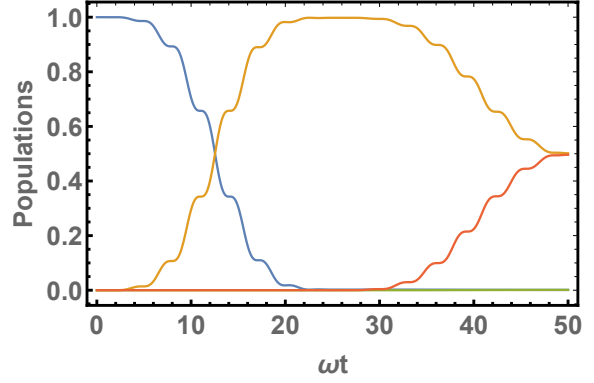
(a) $T = 5/\omega$ (scheme 1)



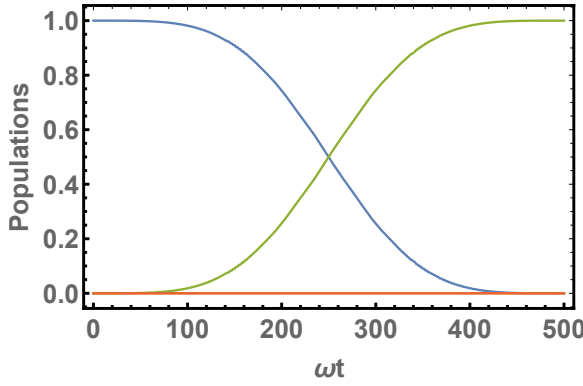
(b) $T = 10/\omega$ (scheme 2)



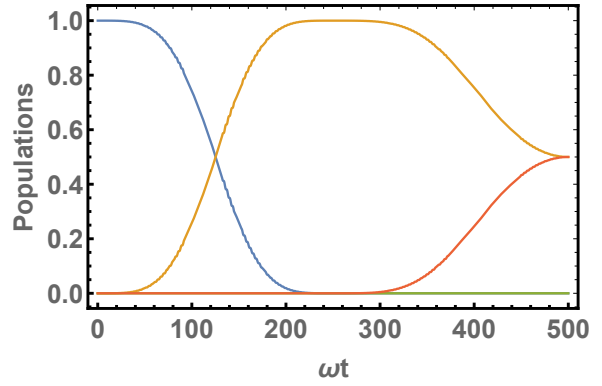
(c) $T = 50/\omega$ (scheme 1)



(d) $T = 50/\omega$ (scheme 2)



(e) $T = 500/\omega$ (scheme 1)



(f) $T = 500/\omega$ (scheme 2)

Figure 12: Comparison of rotating wave approximation in accurate regime and when the assumption breaks down. Subfigures represent state evolution for particle initially in state $|00\rangle$ under influence of (scheme 1) π pulse in Ω_y and (scheme 2) π pulse in Ω_x followed by $\pi/2$ pulse in Ω_y . Legend: $|\langle\psi(t)|00\rangle|^2$ (blue), $|\langle\psi(t)|10\rangle|^2$ (orange), $|\langle\psi(t)|01\rangle|^2$ (green), $|\langle\psi(t)|11\rangle|^2$ (red)

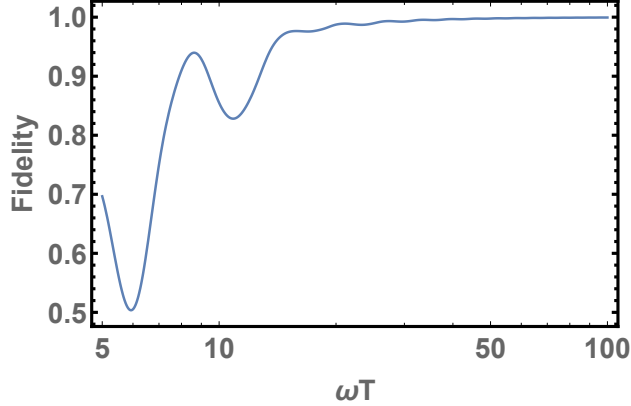


Figure 13: Fidelity $|\langle \Psi_b | \psi(T) \rangle|^2$ dependence on total process time T .

Ω_y with respect to the $|00\rangle \rightarrow |10\rangle$ or $|01\rangle$ transition, an even greater detuning in the $|10\rangle \rightarrow |20\rangle$ or $|01\rangle \rightarrow |02\rangle$ transitions are achieved. This decreases leakage to those states not included in the 4-level approximation and this improves the fidelity of the final state.

Note that it was also assumed that we work in the Mott regime, whereby we discount all interactions between neighbouring lattice sites and thus all overlap integrals (such as γ , the S_{ij} and the C_{ij}) can be taken over the unit cell (assumed to be $x \in [-L, L], y \in [-L, L]$). We have also ignored tunnelling rates and assumed that no tunnelling takes place over timescales of interest (namely, T). In reality tunnelling will take place between lattice sites at a rate defined by the energy of the particles and the properties of the lattice [1]. In the case of the triangular lattice it is an experimentally realised and theoretically predicted fact that tunnelling rates are slow enough to perform the desired observations [22]. The topology of the triangular lattice is such that tunnelling rates may be comparatively lower to that of a square lattice with similar nearest neighbour spacing and particle energy which would improve confinement, but there is the competing effect of more nearest neighbour sites to which an atom may tunnel. The result of these competing effects is a tunnelling rate comparable to that of the square lattice [30] (square) [22] (triangular).

6 Conclusions

We have developed control schemes for the creation of various excited states in a triangular optical lattice using the techniques of (i) lattice shaking, (ii) modulation of polarization phase of the control lasers and (iii) modulation of lattice amplitude. The specific control schemes derived here form only a small subset of the simple states possible in this lattice geometry, but do form part of the basic tools necessary for state preparation in optical lattices. The schemes produced here were all piecewise in nature, but note that invariant-based approaches could be used to optimise the process against certain errors [31]. By optimising the preparation of states against relevant errors such as the leakage to higher resonantly coupled energy states, the fidelity of the final state achieved can be greatly improved.

One important aspect of this work yet to be completed is the numerical simulation of the full Schrödinger equation for the system. This numerical work would confirm the validity of the various approximations and simplifications made in the development of the 4-level schemes. These simulations could be performed via the Fourier split-operator method [32] but this work was not in the scope of this project. In conjunction, an analysis of the tunnelling rates between lattice sites for the various orbitals of interest could be conducted in order to obtain estimations for the lifetimes of the states created in the lattice. When the lattice site occupancy increases past 1, the assumptions made in the derivation of these control schemes are no longer valid (eg. non-interacting particles).

References

- [1] I. Bloch, J. Dalibard, and W. Zwerger, “Many-body physics with ultracold gases,” *Rev. Mod. Phys.*, vol. 80, pp. 885–964, Jul 2008.
- [2] A. M. Rey, “Lecture notes on ultracold atoms in optical lattices,” Summer 2016. https://jila.colorado.edu/arey/sites/default/files/Llecture25_sp_16.pdf.
- [3] P. Soltan-Panahi, J. Struck, P. Hauke, A. Bick, W. Plenkers, G. Meineke, C. Becker, P. Windpassinger, M. Lewenstein, and K. Sengstock, “Multi-component quantum gases in spin-dependent hexagonal lattices,” *Nature Physics*, vol. 7, pp. 434–440, Feb. 2011.
- [4] L. Tarruell, D. Greif, T. Uehlinger, G. Jotzu, and T. Esslinger, “Creating, moving and merging dirac points with a fermi gas in a tunable honeycomb lattice,” *Nature*, vol. 483, pp. 302–305, Mar. 2012.
- [5] G.-B. Jo, J. Guzman, C. K. Thomas, P. Hosur, A. Vishwanath, and D. M. Stamper-Kurn, “Ultracold atoms in a tunable optical kagome lattice,” *Phys. Rev. Lett.*, vol. 108, p. 045305, Jan 2012.
- [6] K. Drese and M. Holthaus, “Ultracold atoms in modulated standing light waves,” *Chemical Physics*, vol. 217, pp. 201–219, May 1997.
- [7] M. Greiner, O. Mandel, T. Esslinger, T. W. Hänsch, and I. Bloch, “Quantum phase transition from a superfluid to a mott insulator in a gas of ultracold atoms,” *Nature*, vol. 415, pp. 39–44, Jan. 2002.
- [8] E. Arimondo, D. Ciampini, A. Eckardt, M. Holthaus, and O. Morsch, “Kilohertz-driven bose–einstein condensates in optical lattices,” in *Advances In Atomic, Molecular, and Optical Physics*, pp. 515–547, Elsevier, 2012.
- [9] A. Alberti, V. V. Ivanov, G. M. Tino, and G. Ferrari, “Engineering the quantum transport of atomic wavefunctions over macroscopic distances,” *Nature Phys.*, vol. 5, p. 547, 2009.
- [10] C. Sias, H. Lignier, Y. P. Singh, A. Zenesini, D. Ciampini, O. Morsch, and E. Arimondo, “Observation of photon-assisted tunneling in optical lattices,” *Phys. Rev. Lett.*, vol. 100, p. 040404, Feb 2008.

- [11] E. Haller, R. Hart, M. J. Mark, J. G. Danzl, L. Reichsöllner, and H.-C. Nägerl, “Inducing transport in a dissipation-free lattice with super bloch oscillations,” *Phys. Rev. Lett.*, vol. 104, p. 200403, May 2010.
- [12] I. Bloch, “Ultracold quantum gases in optical lattices,” *Nature Physics*, vol. 1, pp. 23–30, Oct. 2005.
- [13] X. Li and W. V. Liu, “Physics of higher orbital bands in optical lattices: a review,” *Reports on Progress in Physics*, vol. 79, p. 116401, Sept. 2016.
- [14] A. Isacsson and S. M. Girvin, “Multiflavor bosonic hubbard models in the first excited bloch band of an optical lattice,” *Physical Review A*, vol. 72, Nov. 2005.
- [15] A. B. Kuklov, “Unconventional strongly interacting bose-einstein condensates in optical lattices,” *Physical Review Letters*, vol. 97, Sept. 2006.
- [16] E. Torrontegui, S. Martínez-Garaot, and J. G. Muga, “Hamiltonian engineering via invariants and dynamical algebra,” *Phys. Rev. A*, vol. 89, p. 043408, Apr 2014.
- [17] Y. Tokura, “Orbital physics in transition-metal oxides,” *Science*, vol. 288, pp. 462–468, Apr. 2000.
- [18] S. Maekawa, T. Tohyama, S. E. Barnes, S. Ishihara, W. Koshibae, and G. Khaliullin, *Physics of Transition Metal Oxides*. Springer Berlin Heidelberg, 2004.
- [19] X. Li and W. V. Liu, “Physics of higher orbital bands in optical lattices: a review,” *Reports on Progress in Physics*, vol. 79, p. 116401, sep 2016.
- [20] A. Zenesini, H. Lignier, D. Ciampini, O. Morsch, and E. Arimondo, “Coherent control of dressed matter waves,” *Phys. Rev. Lett.*, vol. 102, p. 100403, Mar 2009.
- [21] D. Daems, A. Ruschhaupt, D. Sugny, and S. Guérin, “Robust quantum control by a single-shot shaped pulse,” *Phys. Rev. Lett.*, vol. 111, p. 050404, Jul 2013.
- [22] C. Becker, P. Soltan-Panahi, J. Kronjäger, S. Dörscher, K. Bongs, and K. Sengstock, “Ultracold quantum gases in triangular optical lattices,” *New Journal of Physics*, vol. 12, p. 065025, June 2010.
- [23] M. Lewenstein, A. Sanpera, and V. Ahufinger, *Ultracold Atoms in Optical Lattices*. Oxford University Press, Mar. 2012.

- [24] F. Gerbier and Y. Castin, “Heating rates for an atom in a far-detuned optical lattice,” *Physical Review A*, vol. 82, July 2010.
- [25] E. Hecht, *Optics 4th ed.*, pp. 386–7. Pearson, 2016.
- [26] J. J. Sakurai, J. J.; Napolitano, *Modern Quantum Mechanics*, p. 67–72. Pearson, 2014.
- [27] A. Kiely, J. G. Muga, and A. Ruschhaupt, “Selective population of a large-angular-momentum state in an optical lattice,” *Physical Review A*, vol. 98, Nov. 2018.
- [28] M. Abramowitz, *Handbook of Mathematical Functions, With Formulas, Graphs, and Mathematical Tables.*. New York, NY, USA: Dover Publications, Inc., 1974.
- [29] A. Kiely, A. Benseny, T. Busch, and A. Ruschhaupt, “Shaken not stirred: creating exotic angular momentum states by shaking an optical lattice,” *Journal of Physics B: Atomic, Molecular and Optical Physics*, vol. 49, p. 215003, Oct. 2016.
- [30] W. Zwerger, “Mott hubbard transition of cold atoms in optical lattices,” *Journal of Optics B: Quantum and Semiclassical Optics*, vol. 5, pp. S9–S16, apr 2003.
- [31] U. Güngördü, Y. Wan, M. A. Fasihi, and M. Nakahara, “Dynamical invariants for quantum control of four-level systems,” *Physical Review A*, vol. 86, Dec. 2012.
- [32] J. A. Fleck, J. R. Morris, and M. D. Feit, “Time-dependent propagation of high energy laser beams through the atmosphere,” *Applied Physics*, vol. 10, pp. 129–160, June 1976.

Appendix A Eigenstate Parity Restriction

Consider the (1D) time independent Schrödinger equation

$$\left[-\frac{\hbar^2}{2m} \frac{d^2}{dx^2} + V(x) \right] \psi(x) = E\psi(x), \quad (\text{A1})$$

where the potential function $V(x)$ is even in x (that is to say $V(-x) = V(x)$). If we reflect the coordinate x to $-x$ and account for the parity of V we are left with

$$\left[-\frac{\hbar^2}{2m} \frac{d^2}{dx^2} + V(x) \right] \psi(-x) = E\psi(-x). \quad (\text{A2})$$

Since both $\psi(x)$ and $\psi(-x)$ solve the same differential equation, we know $\psi(x) = C\psi(-x)$ where C is some constant. Now employing that all wavefunctions must be normalised to be physically realisable, we have that $|C| = 1$ and thus $C = \pm 1$. If we have $\psi(x) = \pm\psi(-x)$, then clearly *all* wavefunctions that solve the time independent Schrödinger equation must be either even or odd.

More heuristically, since the kinetic energy of a particle depends on the square of its momentum and the momentum operator in quantum mechanics describes the curvature of the wavefunction (as it contains a second derivative), we can fairly say that the more “curvy” a wave function is, the higher the energy of the state it represents. Therefore, the more nodes (zeroes) a particular wave function has, the higher the energy. The lowest energy possible state will have no nodes (excluding the fact that it must go to 0 as the coordinates go to infinity) and thus the ground state cannot be odd. If the ground state isn’t odd, we are guaranteed by the above argument that it is even. With each successive state of higher energy, the number of nodes increases by 1 and the parity flips over and back between even and odd. Thus, the first excited state is odd.

Appendix B Eigenstates of Unperturbed Hamiltonian

The unperturbed Hamiltonian H_0 as defined in Eq. 23 is itself not separable in x and y , but the local potential of each unit cell can be approximated by harmonic potentials to obtain estimates of the eigenstates up to fourth order in x and y . The Taylor series of H_0 about $(0, 0)$ is

$$H_0 = \frac{\mathbf{p}^2}{2m} + \frac{3}{2}V_0k^2(x^2 + y^2) + \mathcal{O}(x^4, y^4) \quad (\text{B1})$$

where k represents the *wave number* of the control lasers, as opposed to the usual spring constant. We assume a blue detuning (ie $\Delta > 0$) such that V_0 is positive and therefore the Hamiltonian is locally that of the quantum harmonic oscillator. This approximation becomes more accurate as V_0 increases to the harmonic limit $V_0 \rightarrow \infty$. We have obtained two identical 1D Schrödinger equations, one in x and one in y , whose eigenfunctions are that of the Harmonic potential with effective frequency $\omega^2 = 3V_0k^2/m$. The eigenfunctions of such a potential are well known, with the three lowest energy states given by

$$\Phi_0(s) = \left(\frac{\alpha}{\pi}\right)^{1/4} e^{-\frac{1}{2}\alpha s^2} \quad (\text{B2})$$

$$\Phi_1(s) = \left(\frac{\alpha}{\pi}\right)^{1/4} \sqrt{2\alpha} e^{-\frac{1}{2}\alpha s^2} \quad (\text{B3})$$

$$\Phi_2(s) = \left(\frac{\alpha}{\pi}\right)^{1/4} \left(\frac{2\alpha s^2 - 1}{\sqrt{2}}\right) e^{-\frac{1}{2}\alpha s^2} \quad (\text{B4})$$

in terms of the parameter

$$\alpha = 3k^2 \left(\frac{V_0}{\hbar\omega}\right), \quad (\text{B5})$$

where k is the wavenumber of the control lasers and V_0 is defined by Eq. 5. These approximate eigenfunctions are used in the evaluation of overlap integrals for the purpose of simplifying the 4-level approximations. In the case of Sec. 4.1.3 we have that $\omega_d \rightarrow \omega$ in the harmonic limit $V_0 \rightarrow \infty$, whereas in the case of Sec. 4.2.1 since we are considering second excited states we have $\tilde{\omega}_d \rightarrow 2\omega$ in the harmonic limit. Note that $\tilde{\omega}_d \neq 2\omega_d$ as the spacing in energy levels of the unperturbed Hamiltonian H_0 is not uniform, whereas the spacing of energies in the quantum harmonic oscillator is uniform (and hence the limit of 2ω).

The claim is also made in this report that ground states of H_0 will be even and first excited states is odd. Via Appendix A this is fulfilled if the potential is even in both x and y . Although this Hamiltonian is not separable in x and y , locally the potential is even about 0 in both directions (see Eq. B1).

Appendix C Population Transfer Pulses

Our goal is to transfer a proportion of the population in a given state to another state, provided we have a Hamiltonian H with no diagonal elements (and therefore describes the coupling between basis states). Let us consider a 2-level system described by states $|1\rangle$ and $|2\rangle$ under the action of a Hamiltonian

$$H = \frac{\hbar}{2} \begin{pmatrix} 0 & \Omega \\ \Omega & 0 \end{pmatrix}, \quad (\text{C1})$$

which is represented in the ordered basis

$$|1\rangle = \begin{pmatrix} 1 \\ 0 \end{pmatrix}, \quad |2\rangle = \begin{pmatrix} 0 \\ 1 \end{pmatrix}. \quad (\text{C2})$$

We assume for the moment that Ω is time-independent. Since the eigenstates of H form a basis for the system we may write the time-dependent state of the system $|\Psi(t)\rangle$ in terms of these states as

$$|\Psi\rangle = |1\rangle \langle 1|\Psi\rangle + |2\rangle \langle 2|\Psi\rangle = \begin{pmatrix} \langle 1|\Psi\rangle \\ \langle 2|\Psi\rangle \end{pmatrix} \equiv \begin{pmatrix} \psi_1 \\ \psi_2 \end{pmatrix}. \quad (\text{C3})$$

We can then apply the time-dependent Schrödinger equation $i\hbar \frac{\partial}{\partial t} |\Psi\rangle = H |\Psi\rangle$ to write

$$i\hbar \frac{\partial}{\partial t} \begin{pmatrix} \psi_1 \\ \psi_2 \end{pmatrix} = \frac{\hbar}{2} \begin{pmatrix} 0 & \Omega \\ \Omega & 0 \end{pmatrix} \begin{pmatrix} \psi_1 \\ \psi_2 \end{pmatrix}, \quad (\text{C4})$$

which is a pair of coupled first order differential equations in ψ_1 and ψ_2

$$i \frac{\partial \psi_1}{\partial t} = \frac{\Omega}{2} \psi_2, \quad (\text{C5})$$

$$i \frac{\partial \psi_2}{\partial t} = \frac{\Omega}{2} \psi_1. \quad (\text{C6})$$

This system of equations can be solved by taking the time derivative of one equation and substituting the result into the other to obtain

$$\frac{\partial^2 \psi_1}{\partial t^2} = - \left(\frac{\Omega}{2} \right)^2 \psi_1, \quad (\text{C7})$$

$$\frac{\partial^2 \psi_2}{\partial t^2} = - \left(\frac{\Omega}{2} \right)^2 \psi_2. \quad (\text{C8})$$

If we then impose the boundary conditions that the population is entirely in state $|1\rangle$ at time $t = 0$ such that $\psi_1(t = 0) = 1$, $\psi_2(t = 0) = 0$ and that the total state Ψ is normalized then the solution

to these equations is

$$\psi_1 = \langle 1 | \Psi \rangle = \cos\left(\frac{\Omega}{2}t\right), \quad (\text{C9})$$

$$\psi_2 = \langle 2 | \Psi \rangle = -i \sin\left(\frac{\Omega}{2}t\right). \quad (\text{C10})$$

The probability for the system to be found in the states $|1\rangle$ and $|2\rangle$ are thus given by

$$P_1 \equiv |\langle 1 | \Psi \rangle|^2 = \cos^2\left(\frac{\Omega}{2}t\right), \quad (\text{C11})$$

$$P_2 \equiv |\langle 2 | \Psi \rangle|^2 = \sin^2\left(\frac{\Omega}{2}t\right). \quad (\text{C12})$$

These relations imply that the system oscillates between the states $|1\rangle$ and $|2\rangle$ at a frequency $\Omega/2$. If we allow this Hamiltonian to act on a system initially in the state $|1\rangle$ until such a time that $\Omega t = \pi$, then via Eq. C14 all the population will have been transferred to the state $|2\rangle$. If we then “turn off” the Hamiltonian we have achieved a complete population inversion. This is called a π pulse.

If we instead allow the Hamiltonian to act until such a time that $\Omega t = \pi/2$, then we will have an identical proportion of the population in $|1\rangle$ and $|2\rangle$. Therefore, the system will be in the superposition state

$$|\Psi\rangle = \frac{1}{\sqrt{2}}(|1\rangle - i|2\rangle). \quad (\text{C13})$$

This is called a $\pi/2$ pulse. This can be generalised to a time-dependent Ω in which case we obtain

$$P_1 = |\langle 1 | \Psi \rangle|^2 = \cos^2\left(\frac{1}{2} \int_0^t ds \Omega(s)\right), \quad (\text{C14})$$

$$P_2 = |\langle 2 | \Psi \rangle|^2 = \sin^2\left(\frac{1}{2} \int_0^t ds \Omega(s)\right), \quad (\text{C15})$$

such that the condition for a π pulse becomes $\int_0^t ds \Omega(s) = \pi$ and the condition for a $\pi/2$ pulse becomes $\int_0^t ds \Omega(s) = \pi/2$. The same analysis can be performed in higher dimensions with initial conditions for the occupancy of each basis state in a similar manner, as is applied in the main body of this report.

Appendix D Unitary Transformations

Throughout the body of this report unitary transformations are used to simplify calculations, for example in a reference frame transformation, 4-level approximation and in the removal of a time-dependent energy shift from the Hamiltonian. As quoted in the main text, for a unitary transformation U the Hamiltonian changes as

$$\tilde{H} = U^\dagger H_{\text{old}} U - i\hbar U^\dagger \dot{U} \quad (\text{D1})$$

where \dot{U} represents the partial time derivative of U . What was neglected in the report is the fact that if $\psi(t)$ solves the Schrödinger equation with H_{old} then the new Schrödinger equation with \tilde{H} is solved by the wave function

$$\tilde{\psi}(t) = U\psi(t). \quad (\text{D2})$$

In other words we can write

$$\tilde{H}\tilde{\psi} = i\hbar \frac{d\tilde{\psi}}{dt}. \quad (\text{D3})$$

It would appear then that all target states obtained in the body of the report must include several unitary transformations to be accurate, which is true for all times $0 < t < T$, but by construction all these transformations reduce to the identity \mathbb{I} at the beginning ($t = 0$) and end ($t = T$) of all processes. This is accomplished via the condition that all control parameters are zero-valued at these times. This means that at the beginning and end of all processes the state of the system in our framework which includes several unitary transformations will be identical to the state without these transformations, as the unitary operator acting on a state simply returns the state. The final state will differ from the target state by some global phase, but this does not affect the dynamics of the system and so can be neglected.